Hindawi
Journal of Chemistry
Volume 2023, Article ID 8880213, 20 pages
https://doi.org/10.1155/2023/8880213

Research Article

Docking and Molecular Dynamics Identify Leads against 5 Alpha Reductase 2 for Benign Prostate Hyperplasia Treatment

Selina A. Saah,[1] **Patrick O. Sakyi**,[1,2] **David Adu-Poku**,[1] **Nathaniel O. Boadi**,[3] **Gideon Djan**,[1] **Desmond Amponsah**,[1] **Robert N. O. A. Devine**,[1] **and Kojo Ayittey**[2,4]

[1]*Department of Chemical Sciences, School of Sciences, University of Energy and Natural Resources, P.O. Box 214, Sunyani, Ghana*
[2]*Department of Chemistry, School of Physical and Mathematical Sciences, College of Basic and Applied Sciences, University of Ghana, P.O. Box LG 56, Legon, Accra, Ghana*
[3]*Department of Chemistry, College of Sciences, Kwame Nkrumah University of Science and Technology, PMB, Kumasi, Ghana*
[4]*Science Laboratory Technology Department, Accra Technical University, P.O. Box GP 561, Accra, Ghana*

Correspondence should be addressed to Patrick O. Sakyi; opsakyi@st.ug.edu.gh

Received 28 December 2022; Revised 2 March 2023; Accepted 4 March 2023; Published 28 March 2023

Academic Editor: Fabio Polticelli

Steroid 5 alpha-reductase 2 (5αR-2) is a membrane-embedded protein that together with other isoforms plays a key role in the metabolism of steroids. This enzyme catalyzes the reduction of testosterone to the more potent ligand, dihydrotestosterone (DHT) in the prostate. Androgens, testosterone, and DHT play important roles in prostate growth, development, and function. At the same time, both testosterone and DHT have been implicated in the pathogenesis of benign prostate hyperplasia (BPH). Inhibition of the DHT formation, therefore, provides a therapeutic strategy that offers the possibility of preventing, delaying, or treating BPH. Currently, two steroidal drugs that inhibit 5αR-2, dutasteride and finasteride, have been approved for clinical use. These two come at a high cost and also portray undesirable sexual side effects which necessitate the need to find new chemotherapeutic alternatives for the disease. Based on the aforementioned, finasteride and dutasteride were subjected to scaffold hopping, fragment-based *de novo* design, molecular docking, and molecular dynamics simulations employing databases like ChEMBL, DrugBank, PubChem, ChemSpider, and Zinc15 in the identification of potential hits targeting 5αR-2. Altogether, ten novel compounds targeting 5αR-2 were identified with binding energies lower or comparable to finasteride and dutasteride, the main inhibitors for this target. Molecular docking and molecular dynamics simulations studies identify amino acid residues Glu57, Phe219, Phe223, and Leu224 to be critical for ligand binding and complex stability. The physicochemical and pharmacological profiling suggests the potential of the hit compounds to be drug-like and orally active. Similarly, the quality parameter assessments revealed the hits possess LELP greater than 3 implying their promise as lead-like molecules. The compounds A5, A9, and A10 were, respectively, predicted to treat prostate disorders with Pa (0.188, 0.361, and 0.270) and Pi (0.176, 0.050, and 0.093), while A8 and A9 were found to be associated with BPH treatment with Pa (0.09 and 0.127) and Pi (0.077 and 0.033), respectively. Structural similarity searches via DrugBank identified the drugs faropenem, acemetacin, estradiol valerate, and yohimbine to be useful for BPH treatment suggesting the *de novo* designed ligands as potential chemotherapeutic agents for treating this disease.

1. Introduction

Endocrine processes such as male urine flow, male sexual differentiation of a fetus, male masculinization, anabolism, and libido are mediated by the androgen receptor (AR) [1]. The performance of these diverse functions by AR is achieved by controlling the transcription and expression of specific genes in a ligand-dependent manner in target cells [2]. The ligands that act as transcription factors in these processes are testosterone (T) and dihydrotestosterone (DHT) [1]. 5 alpha-reductase 2 (5αR-2), a member of the membrane-embedded steroid 5α-reductase (SRD5A) family (16), is characterized by seven transmembrane α-helices (7 TMs) connected by 6 loops and located in the membrane of the endoplasmic reticulum [3]. Together with other isoforms, 5αR-2 enhances androgen signaling by reducing

the $\Delta^{4,5}$ double bond of testosterone, the primary androgen in men to the high-affinity agonist DHT using reduced nicotinamide adenine dinucleotide phosphate (NADPH) as a cofactor (Figure 1) [3]. In prostate cells, DHT synchronously stimulates the expression of specific genes; ERG, ETV1, ETV4, PTEN, AR gene, and Bcl-2 are known to facilitate prostate growth and development [4, 5]. Despite being essential to the function of the prostate, DHT also accumulates in prostate cells with age even though in general blood testosterone and DHT levels decline with age [6, 7]. Men suffering from prostate-related urinary symptoms such as benign prostatic hyperplasia (BPH) have higher levels of DHT [8]. BPH is characterized by a noncancerous enlargement of both the stromal and epithelial cells of the prostate gland in the transitional zone [9]. This enlargement blocks the urinary track thereby obstructing the free flow of urine. Pathological evidence of BPH in men has been observed in ~50% of men who are above 50 years old [10]. By age 80, about 83% of men have pathological symptoms of BPH making it an important public health issue [10, 11].

Apart from BPH, the association between the serum balance of androgens with age and its link to prostate cancer risk has become a topic of immense research interest, especially in men above 40 years [12, 13]. In 2018, about 1.3 million new cases were recorded and over 350,000 deaths were as a result of prostate cancer [14]. Interestingly, efforts in probing the etiology and pathogenesis of this malignancy still remain elusive, influencing treatment strategies to be dependent on the risk level portrayed. Classical removal of the prostate (prostatectomy) wholly or partially proved helpful but reports of associated risks including erectile, urinary, and bowel dysfunctions, as well as infertility due to the multifunctional nature of the prostate gland warrant the search for a new treatment alternative [15, 16].

Symptoms of BPH have been alleviated by regulating the production of the transcription factor DHT by blocking the activity of 5αR-2 using synthetic steroids, dutasteride, and finasteride [17]. However, there are reports of associated complications in sexual function after the administration of these drugs which underscores the need for new therapeutics [18, 19]. Computational drug design has however afforded the scientific community with an easy and cost-efficient means of making available chemotypes with improved activity against target proteins [20, 21]. With the limited number of therapeutic agents for BPH treatments coupled with the associated toxicities as well as the increasing rise in the need for new chemotypes, scaffold hopping and fragment-based *de novo* design provide an option in attaining novel compounds with improved activity against 5αR-2. Scaffold hopping which is the identification of new core structures has emerged as one of the techniques toward the discovery of new efficacious drugs. Some examples of drugs designed by scaffold hopping involve the successful development of gamma-aminobutyric acid (GABA) ligands, zopiclone and zolpidem from diazepam [22], cyclooxygenase 2 (COX-2) inhibitors celecoxib and valdecoxib from indomethacin [22, 23], and the antihistamine cyproheptadine inspired from pheniramine [24].

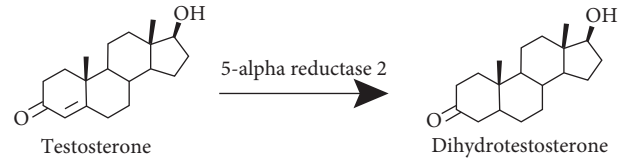

Figure 1: Conversion of testosterone to dihydrotestosterone catalyzed by 5-alpha reductase 2.

Furthermore, fragment-based *de novo* drug design which is the identification of novel chemical structures obtained by linking small molecules with no existing relationship into a drug lead has been explored to keep the drug design pipeline running [25, 26]. Compared to other drug design strategies, *de novo* design explores diverse chemical space and also generates novel therapeutic agents with improved activity against the target of interest [27]. Despite facing synthetic feasibility challenges, of the 59 drugs approved by the US FDA in 2018, 34 of the drugs comprising Asparlas, Braftovi, Copiktra, Crysvita, bautismo, Diacomit, Elzonris, and Epidiolex used for treating rare diseases originated from *de novo* design [28]. This notwithstanding, the *de novo* design of inhibitors against 5αR-2 for BPH treatments is limited. This current work, therefore, seeks to employ scaffold hopping and fragment-based *de novo* design in the identification of nonsteroidal inhibitors targeting 5αR-2. Molecular docking and molecular dynamics simulations studies will then be carried out to elucidate the mechanism of binding and also analyze the stability of the protein–ligand complexes. Finally, absorption, distribution, metabolism, excretion, and toxicity (ADMET) profiling as well as prediction of biological activity will be assessed to identify lead-like molecules.

2. Materials and Methods

The scheme employed in identifying putative hits against 5αR-2 is shown in Figure 2. Finasteride and dutasteride, known inhibitors of 5αR-2 were used for scaffold hopping using a balanced rapid and unrestricted server for extensive ligand-aimed screening (BRUSELAS) [29]. BRUSELAS is a web architecture that employs Weighted Gaussian Algorithm (WEGA), ligand similarity using clique algorithm (LiSiCA), Screen3D, and OptiPharm algorithms to perform shape similarity searching and pharmacophore screening. Structurally similarity search via DrugBank [30], PubChem [31], Zinc15 database [32], and ChemSpider [33] of the identified nonsteroidal ligands from the scaffold hopping was carried out to obtain different structures of each of the core structures. The compendium of chemical entities was then docked to the prepared and energy minimized 5αR-2 (code 7bw1) which was fetched from Research Collaboratory for Structural Bioinformatics Protein Database (RCSB PDB) [34]. Compounds with low binding energy and proper orientation in the binding site were then used for the *de novo* design which were later docked to the protein. The selected novel hit compounds will be evaluated for their ADMET profiles, molecular dynamics simulations, biological activity predictions, and quality parameters computations.

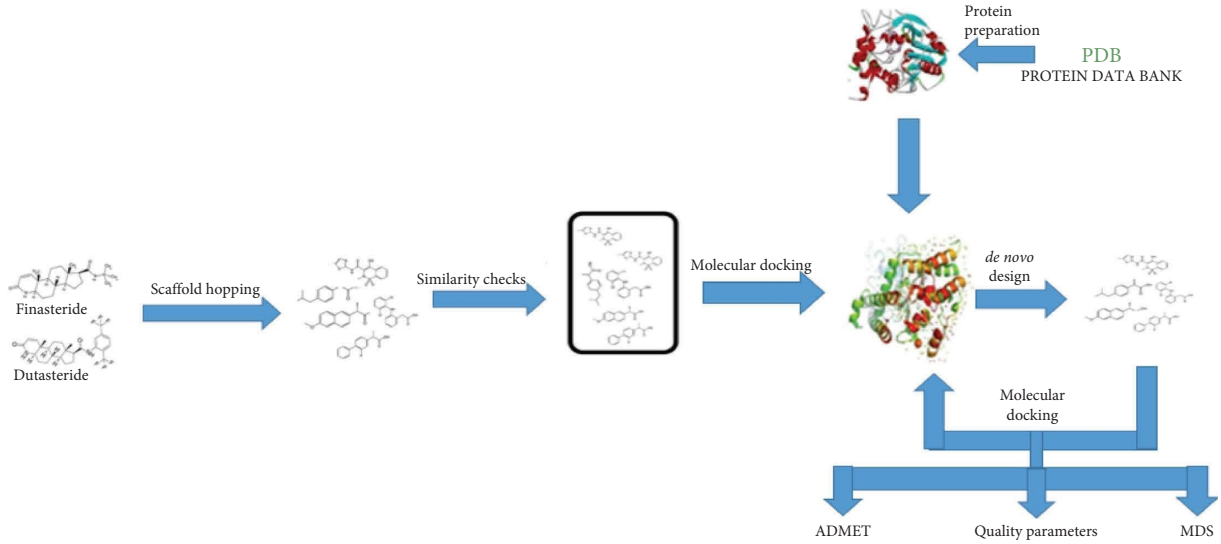

Figure 2: Detailed methodology scheme including scaffold hopping, fragment-based *de novo* design, molecular docking, and molecular dynamics simulations in the identification of potential inhibitors of 5αR-2.

2.1. Receptor Retrieval and Protein Preparation. The solved X-ray crystal structure (PDB code: 7bw1, resolution 2.80 Å) of 5-alpha reductase 2 bound to NADP-finasteride abduct was fetched from RCSB PDB [34]. The probable volume and area of the binding site of the 7bw1 were determined using the Computed Atlas of Surface Topography of proteins (CASTp) [35]. Protein preparation was carried out by first deleting ligands and water molecules using BIOVIA Discovery Studio Visualizer v19.1.0.18287 [36] and then energy minimized employing the optimized potential for liquid simulations (OPLS)/all-atom force field in GROMACS 2018 [37, 38]. The protein was positioned in a cubic simulation box with a 1 nm distance from the edges to restrain particle movements which have the potential of causing effects on the surface atoms [39]. System solvation was carried out using a single point charge and then neutralized to achieve a molarity of 0.15 M using NaCl. The system was energy minimized for 50,000 steps using the steepest descent method. BIOVIA Discovery Studio Visualizer v19.1.0.18287 [36] was used to visualize the energy minimized structure, remove water molecules solvating the protein, and then save in Protein Data Bank (PDB) which was later converted to AutoDock Vina's [40] compatible PDBQT format ready for molecular docking.

2.2. Scaffold Hopping. To find new chemotypes devoid of the steroidal core, the spatial data file (sdf) format of the approved drugs, finasteride and dutasteride, were submitted to the BRUSELAS [29], at a similarity threshold and a set output maximum of 100 scaffolds each. 86 nonsteroidal scaffolds among the 200 generated scaffolds and their structural derivatives fetched from ChemSpider [33], PubChem [31], DrugBank [30], and Zinc15 databases [32] were selected for affinity prediction using AutoDock Vina [40].

2.3. Molecular Docking Studies. The receiver operating characteristic (ROC) curve obtained from easyROC [41] was initially, used to validate AutoDock Vina's ability to differentiate actives from inactives in a library of compounds. To achieve this, the SMILES of finasteride and dutasteride acting as actives served as input for the generation of 50 decoys (inactives) each via the Directory of Useful Decoys (DUD-E) [42].

The molecular docking studies were carried out in two phases using AutoDock Vina [40]. The first phase consisted of a compendium of 4628 compounds comprising the known drugs finasteride, dutasteride and testosterone, dihydrotestosterone, the 86 compounds from BRUSELAS, and their 4538 structural derivatives obtained from the ChemSpider, PubChem, DrugBank, and Zinc databases.

The second phase involved compounds from the *de novo* design. Altogether, the ligands and the protein were prepared using the AutoDock Tools [43] and saved in the input format of AutoDock Vina [40]. The charge, hydrogen bond network, and histidine protonation state of the protein were assigned after PDBQT conversion. The grid box dimension was set to $(-32.131 \times 13.628 \times 19.488)$ Å^3 with the center at (131.579, 80.715, 157.319) Å. Ligands were then virtually screened against the 5αR-2 target protein with exhaustiveness set to the default 8.

2.4. Fragment-Based de novo Design. The protein–ligand complexes from the scaffold hopping served as input into e-LEA3D [44] for the fragment-based *de novo* design with the binding site radius set as 15 Å. With the conformational search, a number of generations, and population size left as default, the final score set was 1 and the same active site coordinates were used as in the molecular docking study. Molecular interactions between hits and 5α*R*-2 were elucidated using BIOVIA discovery studio visualizer v19.1.0.18287 [36].

2.5. Quality Assessment. The ligand efficiency metrics including inhibitory constant, ligand efficiency, ligand efficiency scale, fit quality, and ligand efficiency-dependent lipophilicity were computed as described in previous studies [45, 46].

2.6. ADMET Determination. Toxicity properties of hits were determined using ProTox II [47] and OSIRIS Property Explorer in Data Warrior [48] while their ADME properties were estimated using SwissADME [49].

2.7. Biological Activity Predictions and Exploration of Potential Hit Compounds. The biological activities of the hits were predicted with the simplified molecular input line entry system (SMILES) of the hit compounds using the Prediction of Activity Spectra for Substance (PASS) [50]. DrugBank [30] was screened for structural derivatives to identify drugs that have been used or explored for BPH treatment and possible mechanisms of action from similar compounds.

2.8. Molecular Dynamic Simulation. The stability of each ligand complex was performed using GROMACS version 2018 [37, 38]. A 100 ns molecular dynamics simulation previously described [38] using the GROMOS 43A1 force field was adopted in this study. The unbound protein and protein–ligand complexes were centered in a cubic simulation box with a 1 nm distance from the edges to restrain particle movements which have the potential of distorting the surface atoms [39]. A single point charge was used to solvate the system which was then neutralized to achieve a molarity of 0.15 M using NaCl. Each system was energy minimized for 50,000 steps using the steepest descent method. A 100 ps equilibration was carried out using a number of substances, volume and temperature, and a number of substances, pressure, and temperature ensembles [39] to ensure a well-equilibrated system is achieved at 300 K and a pressure of 1 bar. The root means square deviation (RMSD), radius of gyration (Rg), solvent assessible surface area (SASA), and root mean square fluctuation (RMSF) graphs were generated using QtGrace [51]. Binding free energies of the complexes were calculated using MM-PBSA and the energy contribution of each residue was also determined using g_MMPBSA similar to previous studies [52, 53]. The graphical representation of the MM-PBSA computations was generated using the R programming language [54, 55].

3. Results and Discussion

Presented in this section are the results from the various *in silico* techniques comprising scaffold hopping, *de novo* design, molecular docking and molecular dynamics simulations, ADMET profiling, biological activity predictions, and quality assessment of the identified hit compounds.

3.1. Prediction of Active Site of 5 Alpha Reductase 2. Prediction of the plausible binding residues which constitute the active site of 5αR-2 was done using CASTp [35]. The total active site residues consisted among others (Table 1) Leu16, Leu19, Ala20, Val23, Lys25, Pro26, and Tyr226 making an area of 829.083 Å^2 and a volume of 648.171 Å^3 consistent with a previous study [3].

3.2. Validation of Docking Protocol. Before undergoing docking studies, validation to determine whether AutoDock Vina [40] will be able to distinguish between actives and inactives is predominantly carried out [56, 57]. To accomplish this, AUC was computed from the ROC generated by setting a significant threshold of −7 kcal/mol to differentiate between actives and inactives. Also, Autodock Vina differentiates well between strong binding ligands from their counterparts at this binding energy [58, 59]. The AUC under ROC was evaluated to ascertain the performance of the docking protocol [60]. As a rule of thumb, an AUC of 1 means a perfect classification, and that of 0 is termed an inaccurate classification [61]. Furthermore, an AUC of around 0.9 is classified as outstanding while that of 0.5 suggests no discrimination [45, 61]. The computed AUC under the ROC (Figure 3) for this study was found to be 1 suggesting a perfect classification. A similar study to identify potent inhibitors against *Mycobacterium ulcerans* cystathionine γ-synthase metB observed AutoDock Vina to be able to select actives with a computed AUC of 0.76 during validation of the docking protocol [60]. Compared to the AUC of 1 reported in this work suggests AutoDock Vina will most certainly, discriminate actives from inactives.

3.3. Scaffold Hopping. To identify ligands with new core structures and improved or comparable activity against 5αR-2, scaffold hopping of finasteride and dutasteride using BRUSELAS [29] afforded 200 compounds from the ChEMBL database [62] with varying similarity scores. Virtual screening of the 4538 nonsteroidal compounds against the target protein identified 36 hits which were selected based on how deep they dock into the receptor binding site [59, 63, 64] as well as the binding energy.

The core structures found in the 86 scaffolds included O, N, and S-heterocycles comprising indole, thiazole, isochromene, acridine-1,9-dione, imidazoline-2,4-dione, isoindoline-1,3-dion, pyrazolo[4,3-c]pyridine, pyrido[4,3,b]indole, and 1,38-triazaspiro[4,5]dione. The medicinal properties of these heterocycles have been reported for the treatment of cancer, leishmaniasis, diabetes mellitus, and malaria [65–67]. Among the ten best scoring scaffolds (Supplementary Table 1) to dutasteride, CHEMBL337492 and CHEMBL583325 (Supplementary Table 1) which are epimers of each other with a bis-(trifluoromethyl)benzene moiety were found to show a similarity score of 0.6055 and 0.56708, respectively. Interestingly, most of the scaffold hopping of dutasteride generated ligands with bis-(trifluoromethyl)benzene possibly due to the presence of a similar group on dutasteride. Similarly, CHEMBL1095783 and CHEMBL1410490 with the highest similarity scores of 0.41441 and 0.41287 (Supplementary Table 1), respectively, to finasteride were both found to possess a 1*H*-pyrazole moiety, a *N*-heterocyclic compound known for various therapeutic activities.

Table 1: Predicted binding site residues located within a specific area and volume of 5αR-2.

Pocket	Surface area (Å^2)	Volume (Å^3)	Residues present in the pocket
1	829.083	648.171	Leu16, Leu19, Ala20, Val23, Lys25, Pro26, Ser27, Tyr29, Gly30, Lys31, Ala40, Trp44, Gln47, Glu48, His81, Tyr82, Arg85, Tyr89, Asn93, Arg94, Gly95, Arg96, Tyr98, Leu102, Arg105, Gly106, Phe109, Cys110, Asn151, Asp155, Leu158, Arg159, Leu161, Arg162, Ser168, Tyr169, Arg170, Pro172, Phe177, Ser181, Gly182, Asn184, Phe185, Glu188, Trp192, Phe207, Ser211, Phe214, Leu215, Leu217, Arg218, His221, His222, Tyr226

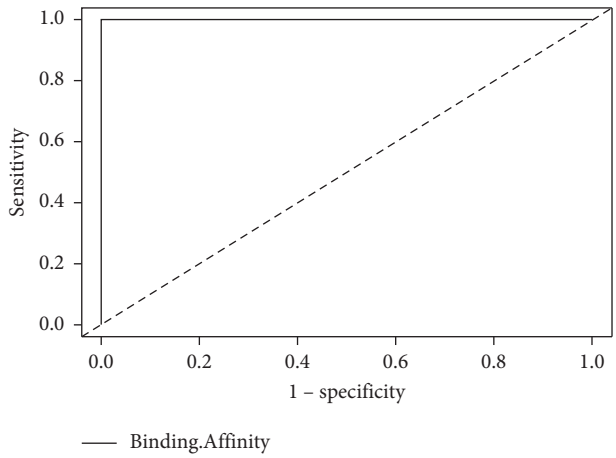

Figure 3: ROC plot generated by screening two active ligands and their decoys to the target protein structure, 5αR-2. The resulting AUC was found to be 1 classified as perfect.

The 10 best hits (Supplementary Table 2) out of the 23 compounds were found to bind deep into the pocket of 5αR-2 and also showed a binding energy lower than the natural substrate, testosterone (−10.2 kcal/mol), and the drug, finasteride (−9.8 kcal/mol) (Supplementary Table 2). Compared to dutasteride (−11.7 kcal/mol), apart from SH8, SH9, and SH10 which showed comparable binding energy to the drug, the rest produced lower binding energies with SH1 and SH2 recording binding energies of −12.8 and −12.6 kcal/mol, respectively (Supplementary Table 2).

3.4. Fragment-Based de novo Design. The linking of small molecules that fit various constraint portions in a binding site of a protein target to form a drug lead is known as fragment-based *de novo* design [68]. Fragment-based *de novo* drug design leads to the identification of novel and potent inhibitors with improved activities against their target of inhibition compared to repurposing [69]. Moreover, the cost- and time-efficient manner of *de novo* design has already yielded leads for the treatment of human ailments including leishmaniasis, bacterial infections, and cancer [45, 46, 69, 70]. However, *de novo* design drugs for BPH treatment are yet to be fully explored hence this research. The possible cytotoxicity of the steroidal core of finasteride and dutasteride on the cholesterol biosynthetic pathway has prompted the need for the production of novel compounds with alternative core structures [45]. Pursuant to this, the 23 compounds obtained from the scaffold hopping with lower or comparable binding energy to finasteride, dutasteride, and testosterone were submitted to e-LEA3D [44] for the *de novo* design. In all, 129 potential novel compounds were generated which were checked for redundancy and also filtered based on Lipinski's rule of five (Ro5). This reduced the dataset to 36 compounds that were subjected to molecular docking studies.

Altogether, 10 compounds (Table 2) were found to dock deep into the binding pocket of 5αR-2 protein and also showed binding energy lower than testosterone (−10.2 kcal/mol) and finasteride (−9.8 kcal/mol). Moreover, the proposed hit compounds recorded lower or comparable binding energy to dutasteride (−11.7 kcal/mol). Amongst the 10 hit compounds, while A1 recorded the lowest binding of −12.9 kcal/mol, compound A10 showed a binding energy of −10.1 kcal/mol. Interestingly, results from docking studies using AutoDock Vina reveal that ligands with binding energy ≤−7.0 kcal/mol to the protein of interest have mostly, gone ahead to show significant biological activity against the target [58, 59, 71]. The recorded binding energy of the hit compounds, therefore, suggests their potential of inhibiting 5αR-2 for BPH treatment. Further search through the public databases including ChemSpider [33], Zinc15 [32], PubChem [31], or DrugBank [30] found no duplicates of these compounds suggesting the uniqueness of the selected hit compounds.

3.5. Characterization of the Binding Interactions. The atomistic studies of protein–ligand interactions have provided the platform for designing hits with the required specificity to the target of interest [72]. The stability of the protein–ligand complexes is dependent on the interactions between the functional groups present on the ligand and amino acid residues in the binding site of the protein [72]. Moreover, the presence of hydrogen bonds and hydrophobic interactions result in the stabilization of the protein–ligand complex [73]. Based on the aforementioned, the two-dimensional (2D) interactions as visualized by Discovery Studio [36] for the protein–ligand complexes revealed the hit compounds to bind with critical amino acids including Leu20, Leu23, Ala24, Trp53, Glu57, Tyr91, Arg94, Tyr98, Phe118, Glu197, Phe219, and Leu224 present in the binding pocket of the 5αR-2 receptor. The interactions present in the protein–ligand complexes included *pi*-anion, *pi*-*pi* stacking, *pi*-alkyl, *pi*-sigma, carbon-hydrogen, and hydrogen bonds.

The elucidation of the structure of 5αR-2 revealed the amino acids Glu57, Trp58, Tyr91, and Arg114 to be critical for the biological activity of the target [3]. The scaffold-hopped ligands were found to interact via hydrogen bonding with at

Table 2: The *de novo* designed hit compounds and the binding energy resulting from the interactions between the amino acids in the pocket of the target protein and the ligand.

Hit compounds	Binding energy (kcal/mol)	Binding residues	
		Hydrogen bonding	Hydrophobic bonding
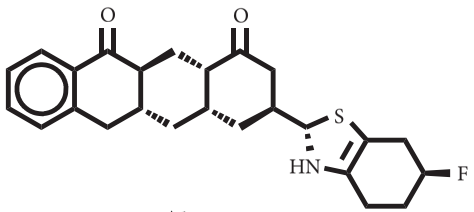 A1	−12.9		Leu20, Trp53, Gly115, Phe118, Phe219, Phe223, Leu224
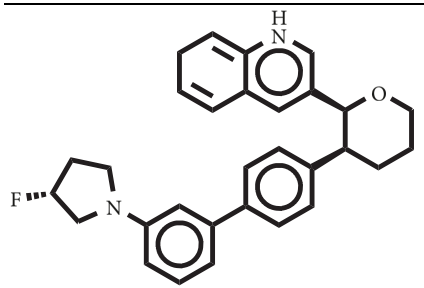 A2	−12.8		Leu20, Ala24, Leu111, Arg114, Phe219, Phe223, Leu224,
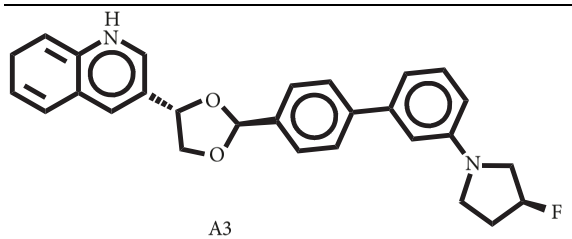 A3	−12.6	Glu197	Leu20, Leu23, Ala24, TRP53, Phe118, Cys119, Phe194, Phe219, Leu224, Phe223
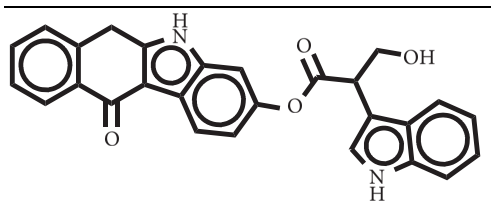 A4	−12.6	Tyr33, Arg94, Tyr98, Asn193	TrpLeu167

Table 2: Continued.

Hit compounds	Binding energy (kcal/mol)	Binding residues	
		Hydrogen bonding	Hydrophobic bonding
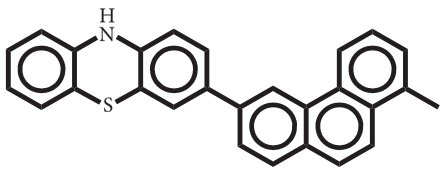 A5	−11.9		Arg134, Leu167, Phe194, Phe223, Leu224
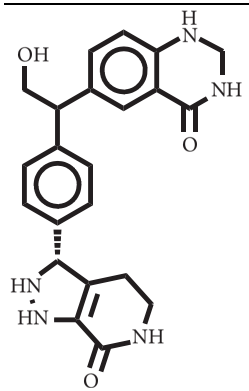 A6	−11.6	Gln56, Asp164, Asn193	Trp53, Phe194, Phe223, Leu224
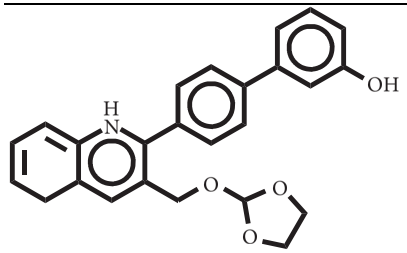 A7	−11.4	Trp53, Asn102, Asp164, Arg179	Gly34, Leu167, Leu170, Tyr178, Phe194

Table 2: Continued.

Hit compounds	Binding energy (kcal/mol)	Binding residues	
		Hydrogen bonding	Hydrophobic bonding
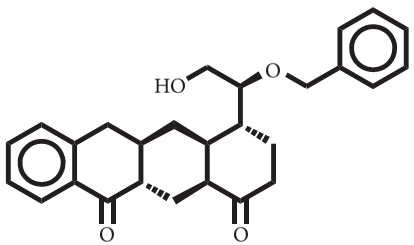 A8	−10.8	Tyr107, Arg114	Leu20, Ala24, Phe118, Phe219, Phe223
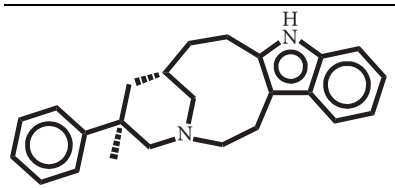 A9	−10.4	Glu57	Leu111, Phe118, Phe223
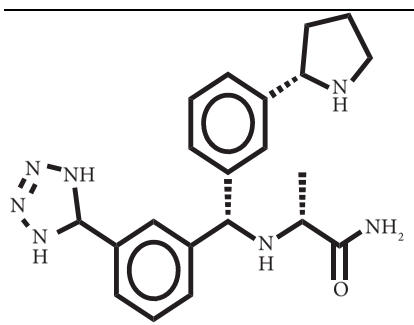 A10	−10.1	Tyr33, Gly34, Trp53, Asn102, Arg105	Tyr98, Leu167, Leu170, Arg171, Tyr178

least one of the amino acids' residues in the binding site of the target. Compared to the known drugs, dutasteride formed three hydrogen bonds (Supplementary Table 2 and Figure S1m) with critical amino acid in the pocket of the target while testosterone and finasteride formed two and one, respectively. The compound SH1 with a binding energy of −12.8 kcal/mol interacted with Tyr98 and Asn193 (Supplementary Table 2 and Figure S1a) through hydrogen bonding. Similarly, hydrogen bonding interaction with Tyr98 (Supplementary Table 2, Supplementary Figures S1d and S1m) enhances the complex stability of SH4 and the dutasteride. Hydrophobic interactions with Phe118, Phe216, Phe219, Phe223, and Leu224 (Supplementary Table 2, Supplementary Figures S1a, S1c–S1e, S1i, and S1j) were observed for the almost all protein-scaffold hopped ligand complexes. As many as six of the scaffold hopped ligands, SH1, SH3, SH4, SH5, SH9, and SH10 were found to possess cyclic or acyclic amide similar to what is present in finasteride and dutasteride acting as either hydrogen bond donor or acceptor. The interactions between this group and binding site residues are the reason for the low binding energies shown to be the complexes.

Furthermore, the *de novo* designed hit compounds exhibited similar interactions as shown by the scaffold-hopped ligands. While A1, A2, and A5 failed to form hydrogen bonding interactions with any amino acid residue in the binding site of the protein, the compounds A3, A4, A6, A7, A8, A9, and A10 formed one, four, three, four, two, one, and five hydrogen bond interactions (Supplementary Figures S2b, S2c, and S2e–S2h), respectively. Interestingly, the hit compounds A8 and A9 interacted via hydrogen bonding with Arg114 and Glu57 (Supplementary Figures S2g and S2h), respectively, similar to other studies which found the two residues to be critical for enzyme inhibition [3]. Compared to the known drug, finasteride formed a hydrogen bonding with Ser74, while testosterone formed a hydrogen bonding with Ser27 and Glu188 (Supplementary Figures S1k and S1l and Supplementary Table 2). Despite not forming any hydrogen bonding, hydrophobic interactions of A1 and A2 with Leu20, Phe219, Phe223, and Leu224 (Table 1, Figure 4, Supplementary Figure S2a) enhance complex stability resulting in a low binding energy of −12.9 and −12.8 kcal/mol, respectively. Similar interactions with the amino acids of the elucidated 5αR-2- abduct resulted in the stability of the complex [3]. Altogether, the *de novo* designed hit compounds were found to form a number of interactions with critical resides by fitting well within the binding pocket of the receptor implying the compounds have the potential of inhibiting 5αR-2.

3.6. ADMET Assessment of Proposed Molecules. Pharmacological and physicochemical profiling assesses the potential of a drug to reach the site of action and stay there long enough to elicit a biological response. Physicochemical profiling evaluated Lipinski's rule of five (Ro5) to determine whether a drug with certain pharmacological or biological activity has the chemical and physical properties to make them orally active. The criteria for orally active drugs include molecular weight (Mw) ≤ 500 Da, LogP ≤ 5, hydrogen bond donors ≤ 5, hydrogen bond acceptors ≤ 10, and 40 ≤ molar refractivity ≤ 140 [74]. SwissADME [49] predicted all the hit compounds to be orally active since they failed to violate any of the rules. Moreover, Veber's rule [75] stipulates that an orally active drug must possess a number of rotatable bonds ≤10 and a polar surface area ≤140 Å^2. The identified hit compounds were found to obey Veber's rule suggesting they possess the potential to be orally active.

Solubility was assessed to predict the dissolution of the hit compounds in the blood to enhance their bioavailability [76]. Recent studies have hinged on solubility prediction as one of the major factors for drug design as many drugs failed clinical trials due to poor solubility [77]. A logS > −6 is the recommended range for the solubility of a potential druggable candidate [78]. Apart from A2 and A5 (Table 3) which were predicted to show poor solubility, the rest recorded moderate to high solubility. Converse to the known drugs, while finasteride was predicted to be soluble, dutasteride exhibited poor solubility. Assessment of bioavailability score (BS) was done to identify the hit compounds which can readily be absorbed. The BS for the hit compounds was computed to be 0.55 (Table 3) similar to previous drug design strategies in the identification of hit compounds [45, 60]. Moreover, gastrointestinal absorption (GI) was evaluated to measure the ability of the hit compounds to be absorbed into the intestines. A druggable candidate is expected to possess a high GI for complete absorption into the bloodstream [79] which is exactly what was predicted for the hit compounds suggesting the potential drug-likeness of the compounds. Surprisingly, dutasteride was predicted to possess low GI while finasteride showed otherwise.

Molar refractivity (MR) was evaluated to give vital information on the pharmacokinetics and pharmacodynamics of the selected hit compounds [80]. The predicted overall polarity of the hit compounds except A3 was within the acceptable MR range of less than 130 Å^2. A good drug candidate should be synthetically feasible to make it available when found to show the right biological activity. The synthetic accessibility (SA) of hit compounds should not be greater than 6 [46, 81, 82] and all the hit compounds and the known drugs were found to have SA lower than 6. Drugs with the propensity to cross the blood-brain barrier (BBB) tend to attach to brain receptors to elicit a biological response [83]. Among the predicted hits, only five that is A3, A4, A5, A6 and A8 (Table 3) possessed the ability to permeate BBB and attached to the brain parenchyma and activate certain receptors. Compared to the controls, while finasteride showed BBB permeation, dutasteride was not. A drug that is a substrate of permeability glycoprotein (P-gp) has the potential of possessing high bioavailability and hence will stay at the active site to elicit a biological effect before being flushed out [45, 84]. Apart from A1 and A2, the remaining eight hit compounds together with finasteride and dutasteride (Table 3) were predicted to be P-gp substrates. Altogether, the results from the pharmacological and physicochemical profiling reveal the potential of the *de novo* designed ligands to be a druggable candidate.

The toxicity assessment of the 10 compounds was evaluated using OSIRIS Data Warrior 5.0.0 [48] and ProTox II [47]. Toxicity determinations and predictions have

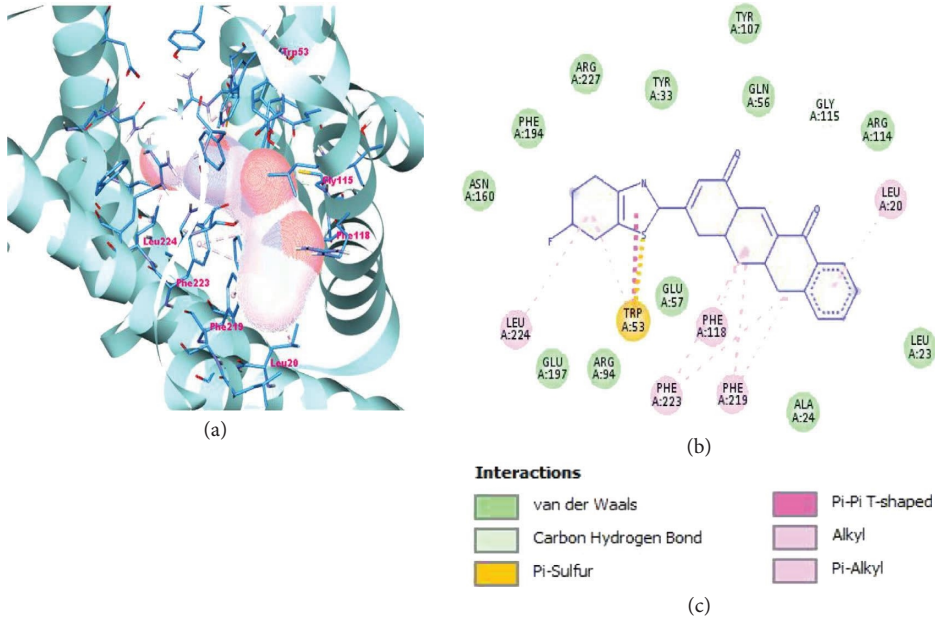

Figure 4: The cartoon representations and 2D interactions of the 5αR-2-hits complexes as visualized in Discovery Studio v19.1.0.18287 [36]: (a) Cartoon of 5αR-2-A1 complex, (b) 2D interaction of 5αR-2-A1 complex, and (c) legend of interactions.

Table 3: Pharmacological and physicochemical profiling of the hit compounds computed molecular weight (MW), number of heavy atoms (NHA), molar refractivity (MR), topological polar surface area (TPSA), gastrointestinal absorption (GI), blood-brain barrier (BBB), number of Ro5 violations (vRoF), bioavailability score (BS), and solubility score (SC).

Compounds	Mw (g/mol)	NHA	MR	TPSA (Å^2)	ClogP	LogS	SC	GI	vRoF	BS	SA	BBB	P-gp
A1	425.56	30	122.03	71.47	4.27	−5.57	Moderate	High	0	0.55	5.56	No	No
A2	454.58	34	140.91	28.26	5.39	−6.45	Poor	High	1	0.55	5.29	No	No
A3	442.52	33	132.38	37.49	4.64	−5.77	Moderate	High	0	0.55	5.14	Yes	Yes
A4	436.46	33	125	95.18	3.95	−5.49	Moderate	High	0	0.55	3.73	No	Yes
A5	389.51	29	128.46	37.33	6.67	−7.96	Poor	Low	1	0.55	3.51	No	Yes
A6	405.45	30	128.74	114.52	0.86	−3.05	Soluble	High	1	0.55	4.59	No	Yes
A7	401.45	30	115.76	63.71	3.79	−4.90	Moderate	High	0	0.55	4.08	Yes	Yes
A8	418.52	31	119.88	63.60	3.81	−4.73	Moderate	High	0	0.55	4.62	Yes	Yes
A9	344.49	26	113.64	19.03	4.67	−5.78	Moderate	High	1	0.55	4.94	Yes	Yes
A10	393.49	29	127.81	115.93	1.86	−3.96	Soluble	High	0	0.55	4.25	No	Yes
Finasteride	372.54	27	113.18	58.2	3.29	−3.86	Soluble	High	0	0.55	5.37	Yes	Yes
Dutasteride	528.53	37	129.94	58.2	5.72	−6.29	Poor	Low	2	0.55	5.36	No	Yes

become critical in drug design to the extent that most drugs have failed to reach clinical trials because they were found to be unsafe [85]. Similarly, some drugs in use have had to be recalled due to reported toxicity issues [86]. The dangers associated with drugs with some levels of toxicities have triggered the recognition of the importance of using multiple *in silico* models in drug risk assessment [87]. Toxicity profiling considered for this study were mutagenicity, tumorigenic, hepatotoxicity, immunotoxicity, cytotoxicity, reproductive effects, and irritants.

Mutagenicity is the ability of a drug to alter the DNA of an organism and as a rule of thumb, administered drugs should not in any way cause this effect. Among the selected hits, only A4 and A5 (Supplementary Table 3) were predicted to be mutagenic. The drugs, finasteride and dutasteride, were predicted to be nonmutagenic. Immunotoxicity is the ability of a compound to alter the functioning of the immune system upon exposure and cause adverse effects. A number of immunotherapeutic agents such as imiquimod, leukinferon, and miltefosine which modulate the host immune systems are already in clinical use for the treatment of human ailments [88–90]. This notwithstanding, a therapeutic agent should not cause adverse modulation of the immune system. The two drugs were predicted to be immunotoxins whereas all the proposed hits were shown to be nonimmunotoxin. Tumorigenecity is the ability of a drug to cause proliferation or induce the proliferation of cancer cells. All the identified hit compounds as well as finasteride and dutasteride (Supplementary Table 3) were predicted not to possess any tumorigenic effects.

Reproductive effects occur when a drug interferes with the ability to produce normal, healthy offspring. A drug causes irritation if it is capable of producing discomfort or phlebitis. Interestingly, with the exception of A4 and A5,

none of the remaining hits and known drugs were predicted to possess any reproductive or irritating effects (Supplementary Table 3). However, erectile dysfunction which deals with the difficulty in getting or maintaining an erection has been associated with the use of finasteride and dutasteride [19, 91].

Cytotoxicity is the harm caused by the action of chemotherapeutic agents on living cells. Cytotoxic compounds have been associated with cell damage or death via necrosis or apoptosis and are applied in the treatment of human diseases including cancer [92]. Though some anticancer agents have been used in treating BPH without affecting healthy cells [93], none of the drugs were shown to possess cytotoxicity effects. However, A4, A5, A7, A8, and A10 (Supplementary Table 3) were predicted to possess low cytotoxicity properties. Hepatotoxicity is an impairment of liver function caused by exposure to xenobiotics and its effect is life-threatening. Results from the predictions show that all the hit compounds were inactive to hepatotoxicity effects compared to finasteride and dutasteride which were predicted to be injurious to the liver. Overall, the predictions indicate that all molecules have a safe pharmacokinetic and pharmacodynamics profile which supports the need for further investigations.

3.7. Biological Activity Predictions and Exploration of Proposed Molecules. The Open Bayesian machine learning algorithm, Prediction of Activity Spectra for Substances (PASS) [50] developed based on the structure-activity relationship (SAR) analysis of the chemical entities present in the database [94] was used to predict the biological activity of the selected molecules (Table 4). From PASS predictions, a ligand with a probability of activity (Pa) > probability of inactivity (Pi) suggests the compound to possess the ability of exhibiting biological activity and hence requires experimental validations [95]. The compounds A1, A2, A3, A4, A5, A6, A7, and A10 were predicted as anticancer compounds with Pa (0.732, 0.215, 0.516, 0.339, 0.192, 0.205, 0.811, and 0.352) and Pi (0.004, 0.068, 0.067, 0.131, 0.055, 0.088, 0.010, and 0.015) (Table 4), respectively. The compounds A2, A3, and A6 showed a similarity score of 0.525, 0.508, and 0.503 with the anticancer agents, zoptarelin doxorubicin, vinblastine, and aldoxorubicin, respectively [96]. Interestingly, the anticancer drugs lycopene [97] and cabazitaxel [98] are already in use for the treatment of BPH in humans [97, 99] suggesting the 5αR-2 inhibitory activities of the proposed molecules. Furthermore, compound A1 shows a similarity score of 0.54 with faropenem, an antibiotic drug used in combination with levofloxacin for BPH treatment [100].

Next, the compounds A3, A4, A5, and A8 were predicted to possess anti-inflammatory properties with Pa (0.403, 0.310, 0.254, and 0.418) and Pi (0.094, 0152, 0.208, and 0.087), respectively. The compound A4 showed a similarity score of 0.574 with acemetacin, a drug for treating pain and inflammation [101]. Consequently, ibuprofen and aspirin, two commonly used nonsteroidal anti-inflammatory drugs, have been shown to decrease viability and suppress the proliferation of BPH cell lines [102]. Similarly, an *in vivo* study revealed that the occurrence of BPH is associated with elevated expressions of cyclooxygenase-2 (COX-2) and 5-lipoxygenase (5-LOX) that regulate inflammation [103]. The prediction of the inflammatory effects of the hit compounds suggests their potential of inhibiting COX-2 and 5-LOX proteins for BPH treatment. Moreover, A8 via DrugBank shows a similarity of 0.549 with estradiol valerate which is used to treat androgen-dependent carcinoma of the prostate [104]. *In vivo* study revealed that mouse-induced BPH had their prostate weight reduced when they were treated with estradiol valerate [105] suggesting the potential of A8 for BPH treatment.

In addition, A5, A9, and A10 were predicted to treat prostate disorders with Pa (0.188, 0.361, and 0.270) and Pi (0.176, 0.050, and 0.093), respectively. Besides A8 and A9 predicted for BPH treatment with Pa (0.09 and 0.127) and Pi (0.077 and 0.033), respectively, they were found to perform this function by inhibiting 5alpha reductase with Pa (0.034 and 0.033) and Pi (0.027 and 0.029), respectively. The known drugs, finasteride and dutasteride used for treating BPH exhibit their mode of action by inhibiting 5alpha reductase 2. Consequently, A9 showed a similarity score of 0.682 with yohimbine, a drug for erectile dysfunction treatment. Interestingly, yohimbine has been found to treat BPH through 5αR-2 inhibition [106] suggesting the potential of A9 to be associated with BPH treatment. Among the ten proposed hits, only A7 was predicted to be associated with alopecia treatment with Pa (0.289) and Pi (0.213) (Table 4). Literature has it that both finasteride and dutasteride are potent drugs for the treatment of alopecia [107, 108]. Overall, the biological activity predictions coupled with the exploration of the compounds in the DrugBank suggest the potential of the *de novo* designed compounds to be promising lead molecules that require experimental validation.

3.8. Evaluation of Quality Parameters. In the time past, affinity has been the criteria for hit selection and optimization [109]. This method suffers drawbacks as affinity tends to be connected with molecular size [109]. Therefore, to assess the potential of the *de novo* designed ligands to be lead molecules, the quality parameters comprising inhibitory constant (K_i), ligand efficiency (LE), ligand efficiency scale (LE_Scale), fit quality (FQ), and ligand efficiency-dependent lipophilicity (LELP) were computed.

The inhibitory constant (K_i) is the concentration required to produce half maximum inhibition and is computed to provide information on the likelihood of a ligand inhibiting the target of interest [110]. The calculations of K_i for all the protein–ligand complexes were obtained using equation (1) similar to an earlier study [45] with slight modification.

$$\ln K_i = \frac{-\Delta G}{0.5924}. \quad (1)$$

A recent *de novo* design of potential inhibitors against *Leishmania donovani* sterol methyltransferase revealed the K_i to be in micro molar [45]. Compared to the results presented in this work, all the calculated K_i were found to be

Table 4: Biological activity predictions of the selected hit compounds using PASS.

Hits	BPH treatment		5alpha reductase inhibitor		Prostate disorder treatment		Anticancer agents		Alopecia treatment		Anti-inflammatory	
	Pa	Pi	Pa	Pi	Pa	Pi	Pa	Pi	Pa	Pi	Pa	Pi
A1	—	—	—	—	—	—	0.732	0.004	—	—	—	—
A2	—	—	—	—	—	—	0.215	0.068	—	—	—	—
A3	—	—	—	—	—	—	0.516	0.067	—	—	0.403	0.094
A4	—	—	—	—	—	—	0.339	0.131	—	—	0.310	0.152
A5	—	—	—	—	0.188	0.176	0.192	0.055	—	—	0.254	0.208
A6	—	—	—	—	—	—	0.205	0.088	—	—	—	—
A7	—	—	—	—	—	—	0.811	0.010	0.289	0.213	—	—
A8	0.090	0.077	0.034	0.027	—	—	—	—	—	—	0.418	0.087
A9	0.127	0.052	0.033	0.029	0.361	0.050	—	—	—	—	—	—
A10	—	—	—	—	0.272	0.093	0.352	0.015	—	—	—	—

in nano molar (Table 5). This suggests the selected hit molecules have the potential of inhibiting 5αR-2.

Ligand efficiency (LE) is the ratio of binding energy to the number of heavy atoms in a ligand and its computation is useful in selecting promising molecules from a library of chemical compounds [111, 112]. Mathematically, LE was calculated using equation (2) where BE is binding energy and NHA is the number of heavy atoms [112].

$$\mathrm{LE} = \frac{-\mathrm{BE}}{\mathrm{NHA}}. \tag{2}$$

For lead-like molecules, the accepted range of values for potential compounds is LE < 0.3 [109]. The proposed hit molecules were however found to have LE > 0.3 (Table 5). This notwithstanding, they still possess the chance of being lead-like as a previous study identified potential drug candidates with LE greater than the threshold [109]. Consequently, lead optimization is likely to reduce the LE to within the acceptable range [109].

To overcome the challenges associated with identifying lead-like molecules based on size-dependent variables, ligand efficiency scaling (LE_Scaling) employs the exponential function in the computation of a ligand to be lead-like [113]. The mathematical relation in equation (3) [45] was used in calculating LE_Scaling where NHA is the number of heavy atoms.

$$\mathrm{LE\_Scaling} = 0.873e^{-0.026\times\mathrm{NHA}} - 0.064. \tag{3}$$

For a ligand to be promising, LE_Scaling is expected to be lower than 0.3. The observed values of LE_Scaling for the *de novo* designed hits were slightly higher than 0.3 except for A2 which recorded LE_Scaling of exactly 0.3 (Table 5). Compared to the control, only A9 (0.380) showed LE_scaling higher finasteride (0.369).

Fit quality (FQ), a parameter dependent on LE_Scaling making it size-independent was computed to measure how firmly the ligand binds in the active site of the target protein [109]. The computation of FQ was evaluated using the expression in the following equation [45, 109]:

$$\mathrm{FQ} = \frac{\mathrm{LE}}{\mathrm{LE\_Scale}}. \tag{4}$$

Table 5: Quality parameters including K_i, LE, Le_Scale, FQ, and LELP for the *de novo* designed hit compounds.

Compound	B.E	K_i (nM)	LE	LE_Scale	FQ	LELP
A1	−12.9	0.349	0.430	0.336	1.280	9.930
A2	−12.8	0.686	0.370	0.300	1.233	14.568
A3	−12.6	1.89	0.360	0.306	1.176	12.889
A4	−12.6	0.686	0.382	0.306	1.248	10.340
A5	−11.9	0.413	0.440	0.347	1.268	15.159
A6	−11.6	3.13	0.390	0.336	1.161	2.205
A7	−11.4	4.39	0.380	0.336	1.131	9.974
A8	−10.8	12.09	0.350	0.326	1.074	10.886
A9	−10.4	23.75	0.400	0.380	1.053	11.175
A10	−10.1	39.41	0.350	0.347	1.009	5.314
Finasteride	−9.8	65.39	0.363	0.369	0.984	9.063

For optimum ligand binding, it is recommended that FQ > 0.8 [109]. The predicted hit molecules and finasteride recorded FQ above 0.8 implying stable protein–ligand complexes.

Ligand-Efficiency-Dependent Lipophilicity (LELP) assesses the potential of a ligand to be lead-like by comparing the binding energy of the compound to lipophilicity [114]. LELP, therefore, adduces the potency of a ligand to binding energy and lipophilicity [114]. The mathematical relation in equation (5) [114] was used for the computation of LELP where logP is the lipophilicity.

$$\mathrm{LELP} = \frac{\log P}{\mathrm{LE}}. \tag{5}$$

For a ligand to be potent and promising, LELP should be greater than 3 [109]. All the selected hit compounds together with finasteride recorded a LELP above 3. This suggests the identified ligands to be potent and hence show promise for BPH treatment targeting 5αR-2.

3.9. Molecular Dynamics Simulations Studies. To ascertain the relative stability of the protein–ligand complexes, 100 ns molecular dynamics simulations were run for the hit compounds with low binding energies (A1, A2, A3, and A4) with finasteride, a known drug for BPH treatment as the control. The RMSD, RMSF, Rg, and SASA trajectories were analyzed in this study. To assess the effects of

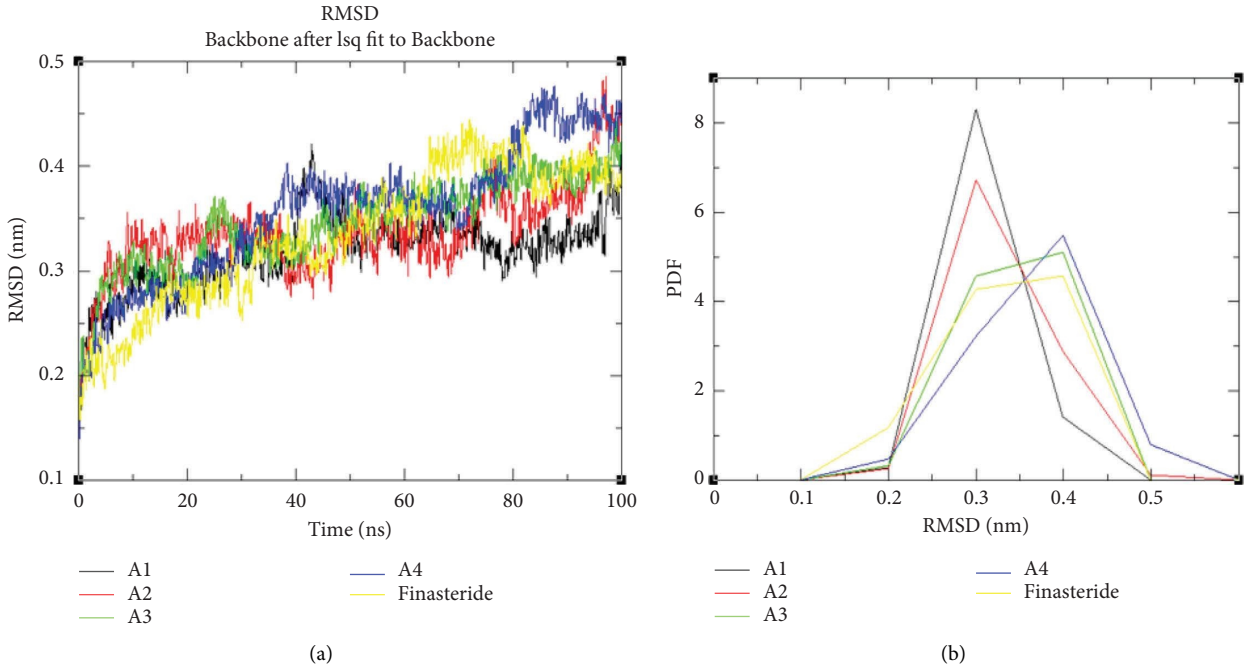

Figure 5: The RMSD analysis of 100 ns trajectory of the protein-hit complexes with finasteride as the control: (a) RMSD for all the complexes; (b) PDF of RMSD for all the complexes.

perturbation on the protein backbone and hence the stability of same [115, 116], the RMSD was determined and plotted. Consequently, from the RMSD plot it was observed that all the complexes including the finasteride attained equilibration between the range 0.3 and 0.5 nm (Figure 5(a)). Moreover, finasteride achieved stability with higher RMSD compared to A4 with the rest of the hit compounds recording low RMSD values. The probability distribution function (PDF) analysis revealed that the finasteride complex attained stability with a RMSD threshold of 0.42 nm (Figure 5(b)) comparable to the A3 and A4. However, the hit compounds A1 and A2 achieved stability with an average RMSD of 0.3 nm (Figure 5(b)) lower than that recorded for finasteride. The lower RMSD of A1 and A2 compared to finasteride, A3 and A4 suggest that the proposed molecules A1 and A2 attained stability with lower RMSD throughout the simulation period. This notwithstanding, overall, the complexes equilibrated and remained stable throughout the simulation.

The interactions between the amino acid residues in the binding site of the protein and ligand result in the stability of the protein–ligand complex [117]. The RMSF which determines the contributions of each amino acid in the binding site to the stability of the complex was measured and plotted. Generally, regions with higher fluctuations in the RMSF plot reveal the amino acids that contributed most towards the stability of the complex [118]. From the RMSF plots, all the complexes including finasteride were observed to show similar trajectories with major fluctuations occurring in the range 40–50, 65–75, 95–105, and 170–180 (Figure 6). This is corroborated by the docking results suggesting amino acid residues within this range to be critical for ligand binding and complex stability. A study to elucidate the structure of

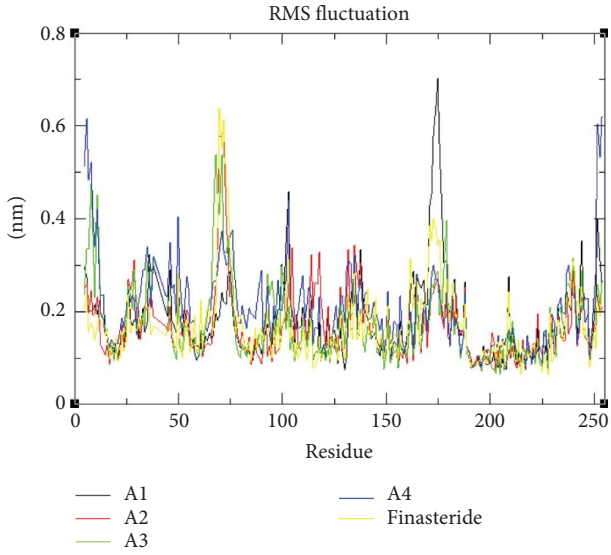

Figure 6: The RMSF analysis of the 100 ns trajectory of the protein-hit complexes with finasteride as the control shows the contributions of the various amino acid residues towards achieving a stable protein–ligand complex.

5αR-2 reveals similar amino acid residues to be responsible for the stability of the 5αR-2-abduct complex [3].

The radius of gyration (Rg) which determines the compactness of the protein–ligand complex [72] was computed and plotted. From the Rg graph, it was observed that while A1 and A2 showed similar trajectories with an average Rg of 1.82 nm, that of A3 and A4 exhibited a similar trend with an average Rg of 1.775 nm (Figure 7(a)). Finasteride, on the other hand, followed the same trajectory

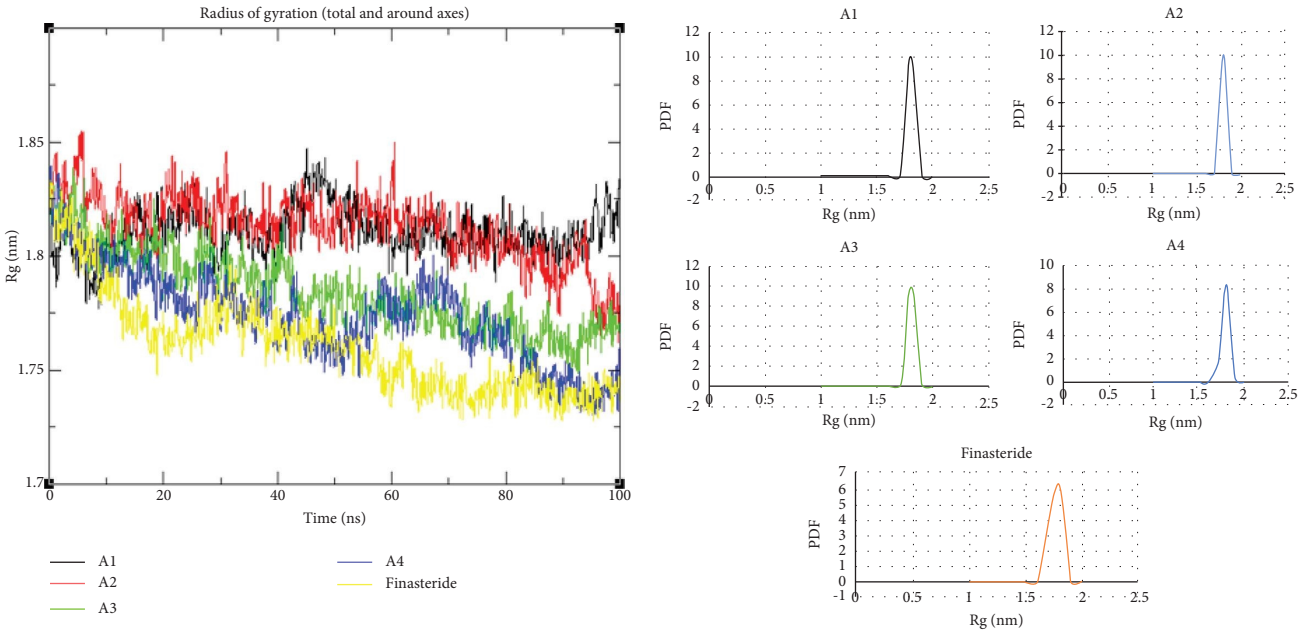

(a) (b)

Figure 7: The Rg analysis of 100 ns molecular dynamics simulations of the hit complexes and finasteride: (a) Rg plot for the four selected complexes; (b) PDF of Rg for the selected lead compounds.

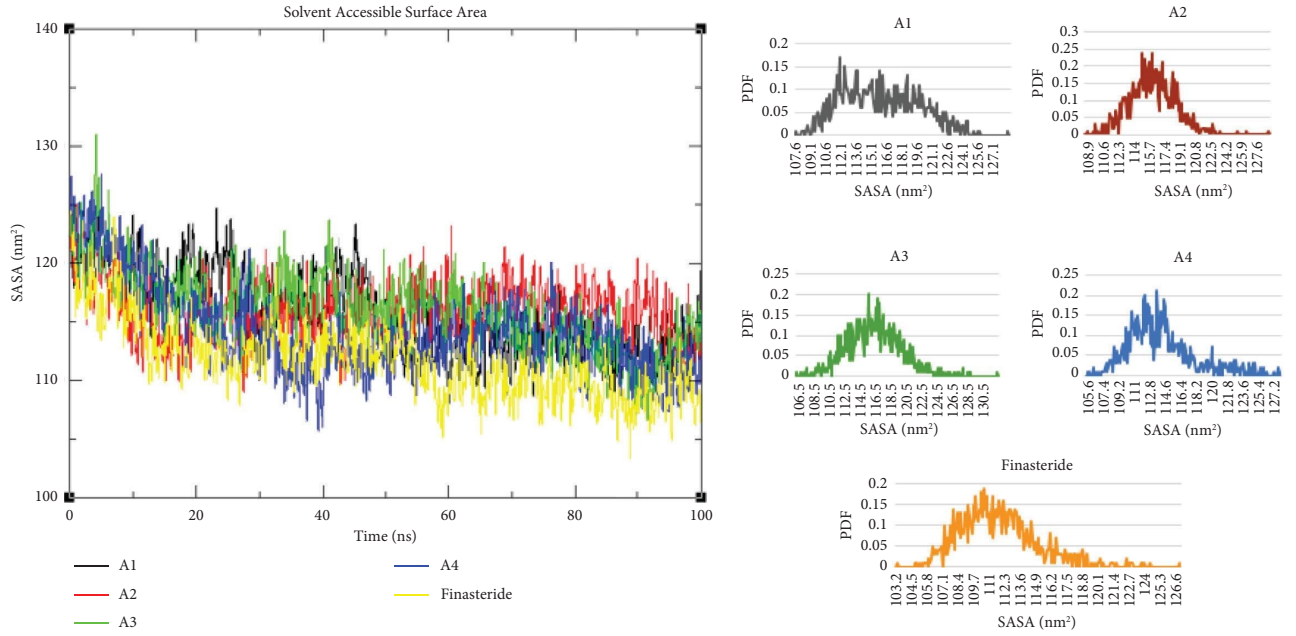

(a) (b)

Figure 8: The SASA analysis of 100 ns molecular dynamics simulations of the hit complexes and finasteride: (a) SASA plot for the four selected complexes; (b) PDF of SASA for the selected lead compounds.

but this time with a lower average Rg of 1.75 nm. Consequently, the PDF analysis revealed that all the complexes including finasteride recorded an average Rg of 1.75 nm (Figure 7(b)) confirming the compactness of the ligands.

Next, solvent accessible surface area (SASA) was evaluated to determine the effects of the solvent behavior on the stability of the protein–ligand complexes [119, 120]. From the SASA graph, it was observed that all the protein–ligand complexes showed similar trajectories with an average SASA value of 115 nm^2 (Figure 8(a)). From the corresponding PDF graph, while finasteride recorded an average SASA of 111.0 nm^2 (Figure 8(b)), the proposed hit molecules showed

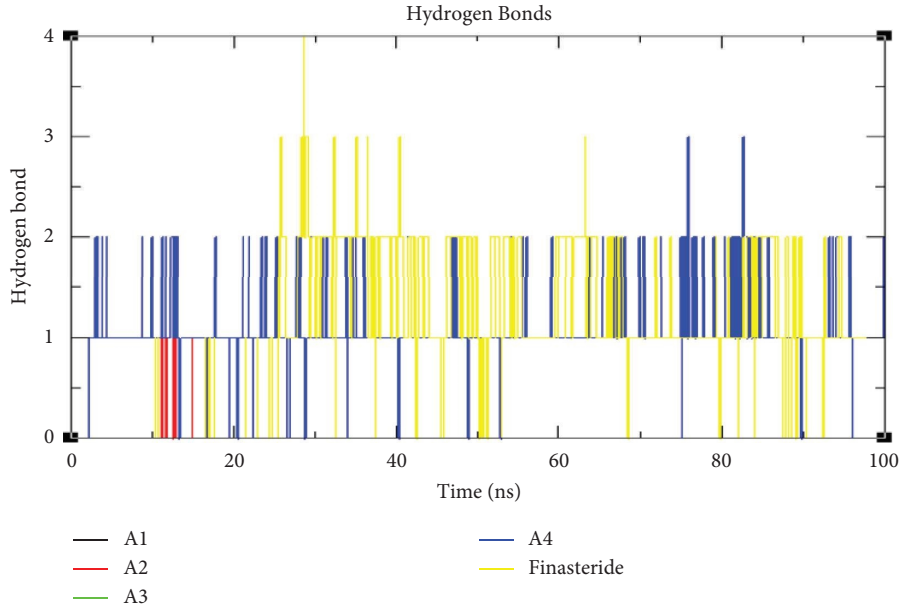

FIGURE 9: The number of hydrogen bond interactions of the protein–ligand complexes during the 100 ns simulations for the five ligands comprising the hits (A1, A2, A3, and A4) and finasteride.

TABLE 6: The van der Waals interactions energy (ΔG_{vdW}), electrostatic energy (ΔG_{ele}), polar solvation energy ($\Delta G_{pol,sol}$), nonpolar solvation energy (ΔG_{SASA}), and free energy of binding (ΔG_{bind}) of the protein–ligand complexes.

Complex	ΔG_{vdW} (kJ/mol)	ΔG_{ele} (kJ/mol)	$\Delta G_{pol,sol}$ (kJ/mol)	ΔG_{SASA} (kJ/mol)	ΔG_{bind} (kJ/mol)
A1	−150.598 ± 6.210	−11.400 ± 2.113	34.786 ± 2.346	−12.528 ± 2.091	−139.740 ± 4.973
A2	−114.398 ± 7.211	−1.077 ± 2.739	15.760 ± 5.281	−10.599 ± 6.910	−110.315 ± 5.521
A3	−168.555 ± 8.002	−6.851 ± 5.755	37.224 ± 3.098	−13.808 ± 7.242	−151.990 ± 6.298
A4	−79.227 ± 7.633	−155.486 ± 4.606	241.903 ± 4.363	−8.055 ± 4.998	−0.865 ± 7.997
Finasteride	−51.518 ± 5.941	−30.599 ± 4.624	46.472 ± 6.810	−4.610 ± 5.099	−40.255 ± 5.940

average SASA values of 112.1, 115.7, 116.5, and 112.8 nm^2 (Figure 8(b)) for A1, A2, A3, and A4, respectively, suggesting the hydrophobic interactions enhanced complex stability for the protein–ligand complexes.

Apart from hydrophobic interactions, hydrogen bonding interactions are known to stabilize protein–ligand complexes. Pursuant to this, the number of hydrogen bonding found to influence the stability of the protein–ligand complexes were computed and plotted. Overall, the number of hydrogen bonding was observed to be between 0–1, 0–2, 0–2, and 0–4 (Figure 9) for A2, A1, A4, and finasteride, respectively. Interestingly, A3 did not record any hydrogen bonding interactions throughout the simulation period suggesting hydrophobic interactions solely, enhancing the complex stability.

3.10. MM-PBSA Calculations for the Evaluation of Potential Leads. The free energy of binding (ΔG_{bind}), van der Waals interactions energy (ΔG_{vdW}), electrostatic energy (ΔG_{ele}), polar solvation energy ($\Delta G_{pol,sol}$), and nonpolar solvation energy (ΔG_{SASA}) associated with the protein–ligand complexes [121, 122] were computed using MM-PBSA technique. Negative free energy of binding signifies an affinity for the ligand towards the protein, hence a high negative ΔG_{bind} implies a stable protein–ligand complex [72, 123]. All the selected hit compounds were shown to possess negative free energy of binding corroborating results from the docking studies suggesting stable protein–ligand complexes. The compound A1 with the lowest binding energy of −12.9 kcal/mol from the docking studies was found to show free energy of binding to be −139.740 kJ/mol lower than finasteride (−40.255 kJ/mol) (Table 6). On the other hand, ligand A3 recorded the lowest free energy of binding of −151.990 kJ/mol compared to the other hit compounds as well as finasteride. Apart from A4 which recorded the highest free energy of binding (Table 6), all the other ligands showed free energy of binding lower than finasteride. In addition, the major contribution to the free energy of binding is in the decreasing order $\Delta G_{vdW} > \Delta G_{ele} > \Delta G_{SASA} > \Delta G_{pol,sol}$. The major contribution of the van der Waals interactions towards the free energy of binding is attributed to possibly the hydrophobic pocket of the target protein.

The energy contribution of each of the amino acid residues toward the stability of the protein–ligand complexes was computed. Generally, binding site residues which contribute energies ≤ -5 kJ/mol and energies $\geq +5$ kJ/mol [124] are suggested to contribute meaningfully to the free energy of binding for the protein–ligand complexes. Among the selected hit compounds, A1 had residues Phe219, Phe223, and

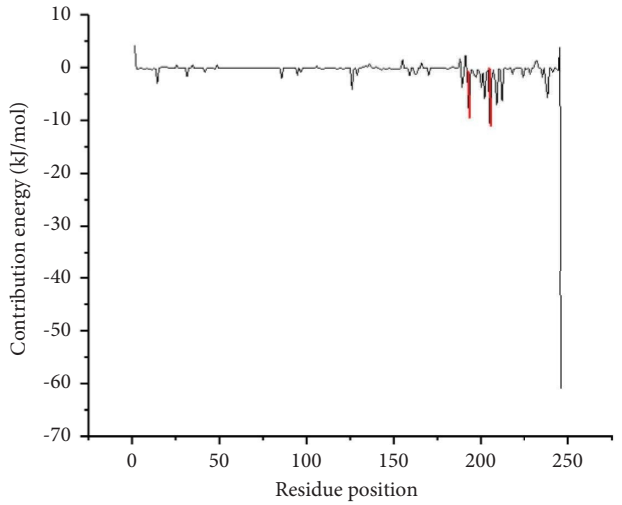

Figure 10: Per-residue energy decomposition trajectory showing the energy contributions of the various amino acid residues towards the stability of the 5αR-2-A1 complex.

Leu224 (Figure 10) contributing the right energies to enhance the stability of the protein–ligand complexes. A similar observation was made for the A2 and A3 which had Phe223 and Leu224 (Supplementary Figures S3a and S3b) contributing energies ≤ -5 kJ/mol or $\geq +5$ kJ/mol for the stability of the complex. Altogether, the majority of the amino acid residues contributed energies that improved the stability of the ligand binding. Particularly, hydrophobic interactions with Phe219, Phe223, and Leu224 and hydrogen bonding with Glu57 enhanced protein–ligand stability which is supported by the results from the docking studies.

4. Conclusion

The number of men especially those with ages above 50 years whose quality of life is impeded due to BPH is increasing at an alarming rate. Surprisingly, the few chemotherapeutic agents available are expensive, scarce, and exhibit worrying toxicity effects. A concerted effort from the drug discovery hub to identify more potent 5αR-2 inhibitors to curtail BPH is urgently needed. Therefore, the current work employed scaffold hopping, fragment-based design, molecular docking, and molecular dynamics simulations in the identification of ten potential 5αR-2 inhibitors. The selected compounds recorded binding energies between -10 and -13 kcal/mol, lower than finasteride but comparable to dutasteride. The results from the docking studies were corroborated with that of molecular dynamics simulations analysis and MM-PBSA calculations identifying amino acid residues Glu57, Phe219, Phe223, and Leu224 to be critical for ligand binding. The physicochemical and pharmacological profiling predicts the compounds to possess the potential to be drug-like with no significant toxicities. Results from the quality parameter calculations show the compounds to be potent and promising as LELP computations for all the hit compounds were found to be greater than 3. Biological activity and exploration predictions espouse the potential of the hit compounds in attenuating 5αR-2 for BPH treatment. The predictions of the hit compounds (A5, A8, and A9) as being associated with BPH and prostate disorder treatments through 5αR-2 inhibition suggest the potential of the ligands and hence warrant experimental authentication.

Data Availability

The data supporting the current study are available from the corresponding author upon request.

Conflicts of Interest

The authors declare that they have no conflicts of interest regarding the manuscript and its contents.

Authors' Contributions

P.O.S and S.A.S conceptualized the project idea. P.O.S, D.A, and G.D. executed all the computational analyses with meaningful contributions from S.A.S, D.A.P, N.O.B, D.N.O.A, K.A, and D.A. P.O.S wrote the first draft after which all the authors read, made their inputs, and finally accepted by all before the manuscript was submitted.

Acknowledgments

The authors are grateful to the West African Centre for Cell Biology of Infectious Pathogens (WACCBIP) and the University of Ghana for making available Zuputo, a DELL high-performance computing system.

Supplementary Materials

Supplementary Table 1 provides the scores of superimposed compounds identified by scaffold hoping of finasteride (in red) and dutasteride (in green). Supplementary Table 2 shows the binding energies and intermolecular interactions between 5αR-2 target protein and the ten predicted scaffolds as well as the known drugs. Supplementary Figure S1 is the 2D interactions of 5αR-2-scaffold hopped ligand complexes (labeled (a) SH1, (b) SH2, (c) SH3, (d) SH4, (e) SH5, (f) SH6, (g) SH7, (h) SH8, (i) SH9, (j) SH10, (k) testosterone, (l) finasteride, and (m) dutasteride) as visualized in Discovery Studio. Supplementary Figure S2 also show the 2D interactions of 5αR-2- *de novo* designed ligand complexes (labeled (a) A2, (b) A3, (c) A4, (d) A5, (e) A6, (f) A7, (g) A8, (h) A9, (i) A10, and (j) legend of interactions) as visualized in Discovery Studio. Supplementary Figure S3 provides the per-residue energy decomposition trajectory showing the energy contributions of the various amino acid residues towards the stability of 5αR-2-ligand (identified as (a) A2, (c) A3, (d) A4, and (e) finasteride) complexes. Supplementary Table 3 shows the toxicity profiles of identified hit compounds as predicted by OSIRIS Data Warrior and ProTox II. (*Supplementary Materials*)

References

[1] S. Hiller-Sturmhöfel and A. Bartke, "The endocrine system: an overview," *Alcohol Health and Research World*, vol. 22, no. 3, pp. 153–164, 1998.

[2] R. A. Davey and M. Grossmann, "Androgen receptor structure, function and Biology: from bench to bedside," *Clinical Biochemist Reviews*, vol. 37, no. 1, pp. 3–15, 2016.
[3] Q. Xiao, L. Wang, S. Supekar et al., "Structure of human steroid 5α-reductase 2 with the anti-androgen drug finasteride," *Nature Communications*, vol. 11, no. 1, p. 5430, 2020.
[4] S. P. Balk and K. E. Knudsen, "AR, the cell cycle, and prostate cancer," *Nuclear Receptor Signaling*, vol. 6, no. 1, p. 06001, 2008.
[5] P. Adamo and M. R. Ladomery, "The oncogene ERG: a key factor in prostate cancer," *Oncogene*, vol. 35, no. 4, pp. 403–414, 2016.
[6] M. Krieg, R. Nass, and S. Tunn, "Effect of aging on endogenous level of 5 alpha-dihydrotestosterone, testosterone, estradiol, and estrone in epithelium and stroma of normal and hyperplastic human prostate," *Journal of Clinical Endocrinology and Metabolism*, vol. 77, no. 2, pp. 375–381, 1993.
[7] K. Welén and J. E. Damber, "Androgens, aging, and prostate health," *Reviews in Endocrine and Metabolic Disorders*, vol. 23, no. 6, pp. 1221–1231, 2022.
[8] T. M. Nicholson and W. A. Ricke, "Androgens and estrogens in benign prostatic hyperplasia: past, present and future," *Differentiation*, vol. 82, no. 4-5, pp. 184–199, 2011.
[9] H. Lepor, "Pathophysiology of lower urinary tract symptoms in the aging male population," *Reviews in Urology*, vol. 7, no. 7, pp. S3–S11, 2005.
[10] A. K. Sauer, H. Vela, G. Vela, P. Stark, E. Barrera-Juarez, and A. M. Grabrucker, "Zinc deficiency in men over 50 and its implications in prostate disorders," *Frontiers Oncology*, vol. 10, p. 1293, 2020.
[11] W. Zhang, X. Zhang, H. Li et al., "Prevalence of lower urinary tract symptoms suggestive of benign prostatic hyperplasia (LUTS/BPH) in China: results from the China Health and Retirement Longitudinal Study," *BMJ Open*, vol. 9, no. 6, Article ID e022792, 2019.
[12] A. Rizzuti, G. Stocker, and H. O. Santos, "Exploring the role of testosterone replacement therapy in benign prostatic hyperplasia and prostate cancer: a review of safety," *Urology*, vol. 2, no. 1, pp. 30–39, 2022.
[13] J. R. Li, S. S. Wang, C. S. Chen et al., "Conventional androgen deprivation therapy is associated with an increased risk of cardiovascular disease in advanced prostate cancer, a nationwide population-based study," *PLoS One*, vol. 17, no. 6, Article ID e0270292, 2022.
[14] R. Huhtaniemi, P. Sipilä, A. Junnila et al., "High intratumoral dihydrotestosterone is associated with antiandrogen resistance in VCaP prostate cancer xenografts in castrated mice," *iScience*, vol. 25, no. 5, Article ID 104287, 2022.
[15] J. K. Rodgers, R. Sawhney, U. Chaudhary, and N. K. Bissada, "Quality of life in men with localized prostate cancer treated by radical prostatectomy or radiotherapy," *Arch Androl*, vol. 52, 2009.
[16] D. P. Smith, M. T. King, S. Egger et al., "Quality of life three years after diagnosis of localised prostate cancer: population based cohort study," *BMJ*, vol. 339, no. 272, p. b4817, 2009.
[17] J. C. Nickel, "Comparison of clinical trials with finasteride and dutasteride," *Reviews in Urology*, vol. 6, no. 9, pp. 1–17, 2004.
[18] T. F. Tsai, G. S. Choi, B. J. Kim et al., "Prospective randomized study of sexual function in men taking dutasteride for the treatment of androgenetic alopecia," *The Journal of Dermatology*, vol. 45, no. 7, pp. 799–804, 2018.
[19] G. Corona, G. Tirabassi, D. Santi et al., "Sexual dysfunction in subjects treated with inhibitors of 5α-reductase for benign prostatic hyperplasia: a comprehensive review and meta-analysis," *Andrology*, vol. 5, no. 4, pp. 671–678, 2017.
[20] K. K. Mak and M. R. Pichika, "Artificial intelligence in drug development: present status and future prospects," *Drug Discovery Today*, vol. 24, no. 3, pp. 773–780, 2019.
[21] S. Pathania, P. K. Singh, R. K. Narang, and R. K. Rawal, "Identifying novel putative ERK1/2 inhibitors via hybrid scaffold hopping –FBDD approach," *Journal of Biomolecular Structure and Dynamics*, vol. 40, no. 15, pp. 6771–6786, 2021.
[22] C. G. Wermuth, P. Ciapetti, B. Giethlen, and P. Bazzini, *Bioisosterism, Compr. Med. Chem. II*, vol. 2, pp. 649–711, 2006.
[23] X. Leval, F. Julemont, V. Benoit, M. Frederich, B. Pirotte, and J.-M. Dogne, "First and second generations of COX-2 selective inhibitors," *Mini-Reviews in Medicinal Chemistry*, vol. 4, no. 6, pp. 597–601, 2004.
[24] H. Sun, G. Tawa, and A. Wallqvist, "Classification of scaffold-hopping approaches," *Drug Discovery Today*, vol. 17, no. 7-8, pp. 310–324, 2012.
[25] C. Gil and A. Martinez, "Is drug repurposing really the future of drug discovery or is new innovation truly the way forward?" *Expert Opinion on Drug Discovery*, vol. 16, no. 8, pp. 829–831, 2021.
[26] V. D. Mouchlis, A. Afantitis, A. Serra et al., "Advances in de novo drug design: from conventional to machine learning methods," *International Journal of Molecular Sciences*, vol. 22, no. 4, pp. 1–22, 2021.
[27] X. Lin, X. Li, and X. Lin, "A review on applications of computational methods in drug screening and design," *Molecules*, vol. 25, no. 6, pp. 1375–1381, 2020.
[28] A. P. P. R. O. V. A. L. S. New Drug Therapy, "FDA," 2019.
[29] A. J. Banegas-Luna, J. P. Cerón-Carrasco, S. Puertas-Martín, and H. Pérez-Sánchez, "BRUSELAS: HPC generic and customizable software architecture for 3D ligand-based virtual screening of large molecular databases," *Journal of Chemical Information and Modeling*, vol. 59, no. 6, pp. 2805–2817, 2019.
[30] D. S. Wishart, Y. D. Feunang, A. C. Guo et al., "DrugBank 5.0: a major update to the DrugBank database for 2018," *Nucleic Acids Research*, vol. 46, no. D1, pp. D1074–D1082, 2018.
[31] S. Kim, J. Chen, T. Cheng et al., "PubChem in 2021: new data content and improved web interfaces," *Nucleic Acids Research*, vol. 49, no. D1, pp. D1388–D1395, 2021.
[32] T. Sterling and J. J. Irwin, "Zinc 15 - ligand discovery for everyone," *Journal of Chemical Information and Modeling*, vol. 55, no. 11, pp. 2324–2337, 2015.
[33] H. E. Pence and A. Williams, "Chemspider: an online chemical information resource," *Journal of Chemical Education*, vol. 87, no. 11, pp. 1123-1124, 2010.
[34] S. K. Burley, H. M. Berman, G. J. Kleywegt, J. L. Markley, H. Nakamura, and S. Velankar, "Protein Data Bank (PDB): the single global macromolecular structure archive," *Methods in Molecular Biology*, vol. 1607, pp. 627–641, 2017.
[35] W. Tian, C. Chen, X. Lei, J. Zhao, and J. Liang, "CASTp 3.0: computed atlas of surface topography of proteins," *Nucleic Acids Research*, vol. 46, no. W1, pp. W363–W367, 2018.
[36] M. Šudomová, S. T. S. Hassan, H. Khan, M. Rasekhian, and S. M. Nabavi, "A multi-biochemical and in silico study on anti-enzymatic actions of pyroglutamic acid against PDE-5, ACE, and urease using various analytical techniques:

unexplored pharmacological properties and cytotoxicity evaluation," *Biomolecules*, vol. 9, pp. 392–405, 2019.

[37] D. Van Der Spoel, E. Lindahl, B. Hess, G. Groenhof, A. E. Mark, and H. J. C. Berendsen, "GROMACS: fast, flexible, and free," *Journal of Computational Chemistry*, vol. 26, no. 16, pp. 1701–1718, 2005.

[38] M. J. Abraham, T. Murtola, R. Schulz et al., "Gromacs: high performance molecular simulations through multi-level parallelism from laptops to supercomputers," *Software*, vol. 1-2, pp. 19–25, 2015.

[39] J. A. Lemkul, "From proteins to perturbed Hamiltonians: a suite of tutorials for the GROMACS-2018 molecular simulation package [article v1.0]," *Living Journal of Computational Molecular Science*, vol. 1, p. 5068, 2019.

[40] O. Trott, A. J. Olson, and A. D. Vina, "AutoDock Vina: improving the speed and accuracy of docking with a new scoring function, efficient optimization, and multithreading," *Journal of Computational Chemistry*, vol. 31, no. 2, pp. 455–461, 2010.

[41] D. Goksuluk, S. Korkmaz, G. Zararsiz, and A. E. Karaagaoglu, "easyROC: an interactive web-tool for ROC curve analysis using R language environment," *The RUSI Journal*, vol. 8, no. 2, pp. 213–230, 2016.

[42] M. M. Mysinger, M. Carchia, J. J. Irwin, and B. K. Shoichet, "Directory of useful decoys, enhanced (DUD-E): better ligands and decoys for better benchmarking," *Journal of Medicinal Chemistry*, vol. 55, no. 14, pp. 6582–6594, 2012.

[43] G. M. Morris, R. Huey, W. Lindstrom et al., "AutoDock4 and AutoDockTools4: a," *Journal of Computational Chemistry*, vol. 30, no. 16, pp. 2785–2791, 2009.

[44] D. Douguet, "e-LEA3D: a computational-aided drug design web server," *Nucleic Acids Research*, vol. 38, pp. 615–621, 2010.

[45] P. O. Sakyi, E. Broni, R. K. Amewu, W. A. I. Miller, M. D. Wilson, and S. K. Kwofie, "Homology modeling, de Novo design of ligands, and molecular docking identify potential inhibitors of Leishmania donovani 24-sterol methyltransferase," *Frontiers in Cellular and Infection Microbiology*, vol. 12, pp. 657–687, 2022.

[46] M. A. Islam and T. S. Pillay, "Identification of promising anti-DNA gyrase antibacterial compounds using de novo design, molecular docking and molecular dynamics studies," *Journal of Biomolecular Structure and Dynamics*, vol. 38, no. 6, pp. 1798–1809, 2020.

[47] P. Banerjee, A. O. Eckert, A. K. Schrey, and R. Preissner, "ProTox-II: a webserver for the prediction of toxicity of chemicals," *Nucleic Acids Research*, vol. 46, no. W1, pp. W257–W263, 2018.

[48] T. Sander, J. Freyss, M. Von Korff, and C. Rufener, "DataWarrior: an open-source program for chemistry aware data visualization and analysis," *Journal of Chemical Information and Modeling*, vol. 55, no. 2, pp. 460–473, 2015.

[49] A. Daina, O. Michielin, and V. Zoete, "SwissADME: a free web tool to evaluate pharmacokinetics, drug-likeness and medicinal chemistry friendliness of small molecules," *Scientific Reports*, vol. 7, no. 1, Article ID 42717, 2017.

[50] A. Lagunin, A. Stepanchikova, D. Filimonov, and V. Poroikov, "PASS: prediction of activity spectra for biologically active substances," *Bioinformatics*, vol. 16, no. 8, pp. 747-748, 2000.

[51] P. Turner, "Grace-5.1. 22/qtGrace v 0.2. 4," 2018, https://plasma-gate.weizmann.ac.il/Grace/doc/UsersGuide.html.

[52] P. O. Sakyi, E. Broni, R. K. Amewu, W. A. Miller, M. D. Wilson, and S. K. Kwofie, "Targeting Leishmania donovani sterol methyltransferase for leads using pharmacophore modeling and computational molecular mechanics studies," *Informatics in Medicine Unlocked*, vol. 37, Article ID 101162, 2023.

[53] P. O. Sakyi, S. K. Kwofie, J. K. Tuekpe et al., "Inhibiting Leishmania donovani sterol methyltransferase to identify lead compounds using molecular modelling," *Pharmaceuticals*, vol. 16, no. 3, p. 330, 2023.

[54] R. R Core Team, *A Language and Environment for Statistical Computing*, R Found. Stat. Comput, Beijing China, 2019.

[55] A. F. M. Alkarkhi and W. A. A. Alqaraghuli, "R Statistical Software," *Appl. Stat. Environ. Sci. with R*, vol. 1, 2020.

[56] S. Kwofie, E. Broni, F. Yunus et al., "Molecular docking simulation studies identifies potential natural product derived-antiwolbachial compounds as filaricides against onchocerciasis," *Biomedicines*, vol. 9, no. 11, p. 1682, 2021.

[57] F. Rahman, S. Tabrez, R. Ali et al., "Virtual screening of natural compounds for potential inhibitors of Sterol C-24 methyltransferase of Leishmania donovani to overcome leishmaniasis," *Journal of Cellular Biochemistry*, vol. 122, no. 9, pp. 1216–1228, 2021.

[58] M. W. Chang, W. Lindstrom, A. J. Olson, and R. K. Belew, "Analysis of HIV wild-type and mutant structures via in silico docking against diverse ligand libraries," *Journal of Chemical Information and Modeling*, vol. 47, no. 3, pp. 1258–1262, 2007.

[59] E. Broni, S. K. Kwofie, S. O. Asiedu, W. A. Miller, and M. D. Wilson, "A molecular modeling approach to identify potential antileishmanial compounds against the cell division cycle (cdc)-2-Related kinase 12 (CRK12) receptor of Leishmania donovani," *Biomolecules*, vol. 11, no. 3, 2021.

[60] S. K. Kwofie, N. N. O. Dolling, E. Donkoh et al., "Pharmacophore-guided identification of natural products as potential inhibitors of mycobacterium ulcerans cystathionine γ-synthase metb," *Computation*, vol. 9, no. 3, pp. 32–24, 2021.

[61] C. Calì and M. Longobardi, "Some mathematical properties of the ROC curve and their applications," *Ricerche di Matematica*, vol. 64, 2020.

[62] M. Davies, M. Nowotka, G. Papadatos et al., "ChEMBL web services: streamlining access to drug discovery data and utilities," *Nucleic Acids Research*, vol. 43, no. W1, pp. 612–620, 2015.

[63] R. Krivák and D. Hoksza, "Improving protein-ligand binding site prediction accuracy by classification of inner pocket points using local features," *Journal of Cheminformatics*, vol. 7, pp. 12-13, 2015.

[64] S. Kumar, P. P. Sharma, U. Shankar et al., "Discovery of new hydroxyethylamine analogs against 3CLproProtein target of SARS-CoV-2: molecular docking, molecular dynamics simulation, and structure-activity relationship studies," *Journal of Chemical Information and Modeling*, vol. 60, no. 12, pp. 5754–5770, 2020.

[65] R. K. Amewu, P. O. Sakyi, D. Osei-safo, and I. Addae-Mensah, "Synthetic and naturally occurring heterocyclic anticancer compounds with multiple biological targets," *Molecules*, vol. 26, no. 23, pp. 7134–7134/48, 2021.

[66] P. O. Sakyi, R. K. Amewu, R. N. O. A. Devine, E. Ismaila, W. A. Miller, and S. K. Kwofie, "The search for putative hits in combating leishmaniasis: the contributions of natural products over the last decade," *Natural Products and Bioprospecting*, vol. 11, no. 5, pp. 489–544, 2021.

[67] U. Farwa and M. A. Raza, "Heterocyclic compounds as a magic bullet for diabetes mellitus: a review," *RSC Advances*, vol. 12, no. 35, pp. 22951–22973, 2022.

[68] M. J. Wasko, K. A. Pellegrene, J. D. Madura, and C. K. Surratt, "A role for fragment-based drug design in developing novel lead compounds for central nervous system targets," *Frontiers in Neurology*, vol. 6, p. 197, 2015.

[69] D. A. Erlanson, "Introduction to Fragment-Based Drug Discovery," *Fragment-based drug discovery and X-ray crystallography*, vol. 2, pp. 1–32, 2011.

[70] W. Cui, A. Aouidate, S. Wang, Q. Yu, Y. Li, and S. Yuan, "Discovering anti-cancer drugs via computational methods," *Frontiers in Pharmacology*, vol. 11, p. 733, 2020.

[71] S. Tabrez, F. Rahman, R. Ali et al., "Repurposing of FDA-approved drugs as inhibitors of sterol C-24 methyltransferase of Leishmania donovani to fight against leishmaniasis," *Drug Development Research*, vol. 82, no. 8, pp. 1154–1161, 2021.

[72] X. Du, Y. Li, Y. L. Xia et al., "Insights into protein–ligand interactions: mechanisms, models, and methods," *International Journal of Molecular Sciences*, vol. 17, no. 2, p. 144, 2016.

[73] R. Patil, S. Das, A. Stanley, L. Yadav, A. Sudhakar, and A. K. Varma, "Optimized hydrophobic interactions and hydrogen bonding at the target-ligand interface leads the pathways of drug-designing," *PLoS One*, vol. 5, no. 8, Article ID e12029, 2010.

[74] C. A. Lipinski, "Lead- and drug-like compounds: the rule-of-five revolution," *Drug Discovery Today: Technologies*, vol. 1, no. 4, pp. 337–341, 2004.

[75] D. F. Veber, S. R. Johnson, H. Y. Cheng, B. R. Smith, K. W. Ward, and K. D. Kopple, "Molecular properties that influence the oral bioavailability of drug candidates," *Journal of Medicinal Chemistry*, vol. 45, no. 12, pp. 2615–2623, 2002.

[76] J. van den Anker, M. D. Reed, K. Allegaert, and G. L. Kearns, "Developmental changes in pharmacokinetics and pharmacodynamics," *The Journal of Clinical Pharmacology*, vol. 58, pp. S10–S25, 2018.

[77] B. Das, A. T. Baidya, A. T. Mathew, A. K. Yadav, and R. Kumar, "Structural modification aimed for improving solubility of lead compounds in early phase drug discovery," *Bioorganic and Medicinal Chemistry*, vol. 56, Article ID 116614, 2022.

[78] C. Fink, D. Sun, K. Wagner et al., "Evaluating the role of solubility in oral absorption of poorly water-soluble drugs using physiologically-based pharmacokinetic modeling," *Clinical Pharmacology and Therapeutics*, vol. 107, no. 3, pp. 650–661, 2020.

[79] R. Löbenberg, G. L. Amidon, H. G. Ferraz, and N. Bou-Chacra, "Mechanism of gastrointestinal drug absorption and application in therapeutic drug delivery," *Ther. Deliv. Methods A Concise Overv. Emerg. Areas*, vol. 23, 2013.

[80] R. T. Sawale, T. M. Kalyankar, R. George, and S. D. Deosarkar, "Molar refraction and polarizability of antiemetic drug 4-amino-5-chloro-N-(2-(diethylamino) ethyl)-2 methoxybenzamide hydrochloride monohydrate in {Aqueous-Sodium or lithium chloride} solutions at 30 o C," *Journal of Applied Pharmaceutical Science*, vol. 6, pp. 120–124, 2016.

[81] L. R. de Souza Neto, J. T. Moreira-Filho, B. J. Neves et al., "In silico strategies to support fragment-to-lead optimization in drug discovery," *Frontiers of Chemistry*, vol. 8, p. 93, 2020.

[82] Q. Huang, L. L. Li, and S. Y. Yang, "PhDD: a new pharmacophore-based de novo design method of drug-like molecules combined with assessment of synthetic accessibility," *Journal of Molecular Graphics and Modelling*, vol. 28, no. 8, pp. 775–787, 2010.

[83] W. A. Banks, "Characteristics of compounds that cross the blood-brain barrier," *BMC Neurology*, vol. 9, no. 1, p. S3, 2009.

[84] V. Prachayasittikul and V. Prachayasittikul, "P-glycoprotein transporter in drug development," *EXCLI J*, vol. 15, pp. 113–118, 2016.

[85] G. A. Van Norman, "Phase II trials in drug development and adaptive trial design," *Journal of the American College of Cardiology: Basic to Translational Science*, vol. 4, no. 3, pp. 428–437, 2019.

[86] I. J. Onakpoya, C. J. Heneghan, and J. K. Aronson, "Post-marketing withdrawal of 462 medicinal products because of adverse drug reactions: a systematic review of the world literature," *BMC Medicine*, vol. 14, pp. 10-11, 2016.

[87] K. T. Rim, "In silico prediction of toxicity and its applications for chemicals at work," *Toxicology and Environmental Health Sciences*, vol. 12, no. 3, pp. 191–202, 2020.

[88] M. Ghosh, K. Roy, and S. Roy, "Immunomodulatory effects of antileishmanial drugs," *Journal of Antimicrobial Chemotherapy*, vol. 68, no. 12, pp. 2834–2838, 2013.

[89] I. Arevalo, G. Tulliano, A. Quispe et al., "Role of imiquimod and parenteral meglumine antimoniate in the initial treatment of cutaneous leishmaniasis," *Clinical Infectious Diseases*, vol. 44, no. 12, pp. 1549–1554, 2007.

[90] O. P. Singh and S. Sundar, "Immunotherapy and targeted therapies in treatment of visceral leishmaniasis: current status and future prospects," *Frontiers in Immunology*, vol. 5, p. 296, 2014.

[91] S. Lee, Y. B. Lee, S. J. Choe, and W. S. Lee, "Adverse sexual effects of treatment with finasteride or dutasteride for male androgenetic alopecia: a systematic review and meta-analysis," *Acta Dermato-Venereologica*, vol. 99, no. 1, pp. 12–17, 2019.

[92] A. Zyad, I. Leouifoudi, M. Tilaoui, H. A. Mouse, M. Khouchani, and A. Jaafari, "Natural products as cytotoxic agents in chemotherapy against cancer," *Cytotoxicity*, vol. 10, 2018.

[93] J. Perez, M. Fuertes, P. Nguewa, J. Castilla, and C. Alonso, "Anticancer compounds as leishmanicidal drugs: challenges in chemotherapy and future perspectives," *Current Medicinal Chemistry*, vol. 15, no. 5, pp. 433–439, 2008.

[94] S. Parasuraman, "Prediction of activity spectra for substances," *Journal of Pharmacology and Pharmacotherapeutics*, vol. 2, no. 1, pp. 52-53, 2011.

[95] M. Kulkarni, M. Basanagouda, V. Jadhav, and R. Rao, "Computer aided prediction of biological activity spectra: study of correlation between predicted and observed activities for coumarin-4-acetic acids," *Indian Journal of Pharmaceutical Sciences*, vol. 73, no. 1, pp. 88–92, 2011.

[96] N. Hanke, M. Teifel, D. Moj et al., "A physiologically based pharmacokinetic (PBPK) parent-metabolite model of the chemotherapeutic zoptarelin doxorubicin-integration of in vitro results, Phase I and Phase II data and model application for drug-drug interaction potential analysis," *Cancer Chemotherapy and Pharmacology*, vol. 81, no. 2, pp. 291–304, 2018.

[97] D. Ilic and M. Misso, "Lycopene for the prevention and treatment of benign prostatic hyperplasia and prostate cancer: a systematic review," *Maturitas*, vol. 72, no. 4, pp. 269–276, 2012.

[98] C. K. Tsao, E. Cutting, J. Martin, and W. K. Oh, "The role of cabazitaxel in the treatment of metastatic castration-resistant prostate cancer," *Therapeutic Advances in Urology*, vol. 6, no. 3, pp. 97–104, 2014.

[99] Z. J. Yu, H. L. Yan, F. H. Xu et al., "Efficacy and side effects of drugs commonly used for the treatment of lower urinary tract symptoms associated with benign prostatic hyperplasia," *Frontiers in Pharmacology*, vol. 11, p. 658, 2020.

[100] T. Muratani, K. Iihara, T. Nishimura et al., "[Faropenem 300 mg 3 times daily versus levofloxacin 100 mg 3 times daily in the treatment of urinary tract infections in patients with neurogenic bladder and/or benign prostatic hypertrophy]," *Kansenshogaku Zasshi*, vol. 76, no. 11, pp. 928–938, 2002.

[101] R. A. Moore, S. Derry, and H. J. McQuay, "Single dose oral acemetacin for acute postoperative pain in adults," *Cochrane Database of Systematic Reviews*, vol. 2009, no. 3, Article ID CD007589, 2009.

[102] C. H. Minnery and R. H. Getzenberg, "Benign prostatic hyperplasia cell line viability and modulation of jm-27 BY doxazosin and ibuprofen," *The Journal of Urology*, vol. 174, no. 1, pp. 375–379, 2005.

[103] H. Ishiguro and T. Kawahara, "Nonsteroidal anti-inflammatory drugs and prostatic diseases," *BioMed Research International*, vol. 2014, Article ID 436123, 6 pages, 2014.

[104] B. Montgomery, P. S. Nelson, R. Vessella, T. Kalhorn, D. Hess, and E. Corey, "Estradiol suppresses tissue androgens and prostate cancer growth in castration resistant prostate cancer," *BMC Cancer*, vol. 10, pp. 244–247, 2010.

[105] C. E. C. C. Ejike and L. U. S. Ezeanyika, "Management of experimental benign prostatic hyperplasia in rats using a food-based therapy containing Telfairia occidentalis seeds," *African Journal of Traditional, Complementary and Alternative Medicines: AJTCAM*, vol. 8, no. 4, pp. 398–404, 2011.

[106] Y. Zhao, Y. Zhang, Y. Li et al., "Yohimbine hydrochloride inhibits benign prostatic hyperplasia by downregulating steroid 5α-reductase type 2," *Eur J Pharmacol*, vol. 908, Article ID 174334, 2021.

[107] K. J. McClellan and A. Markham, "Finasteride: a review of its use in male pattern hair loss," *Drugs*, vol. 57, no. 1, pp. 111–126, 1999.

[108] T. Arif, K. Dorjay, M. Adil, and M. Sami, "Dutasteride in androgenetic alopecia: an update," *Current Clinical Pharmacology*, vol. 12, no. 1, pp. 31–35, 2017.

[109] S. Schultes, C. De Graaf, E. E. J. Haaksma, I. J. P. De Esch, R. Leurs, and O. Krämer, "Ligand efficiency as a guide in fragment hit selection and optimization," *Drug Discovery Today: Technologies*, vol. 7, no. 3, pp. e157–e162, 2010.

[110] G. A. Holdgate, T. D. Meek, and R. L. Grimley, "Mechanistic enzymology in drug discovery: a fresh perspective," *Nature Reviews Drug Discovery*, vol. 17, 2018.

[111] A. L. Hopkins, C. R. Groom, and A. Alex, "Ligand efficiency: a useful metric for lead selection," *Drug Discovery Today*, vol. 9, no. 10, pp. 430-431, 2004.

[112] C. Abad-Zapatero, O. Perišic, J. Wass et al., "Ligand efficiency indices for an effective mapping of chemico-biological space: the concept of an atlas-like representation," *Drug Discovery Today*, vol. 15, no. 19-20, pp. 804–811, 2010.

[113] C. H. Reynolds, S. D. Bembenek, and B. A. Tounge, "The role of molecular size in ligand efficiency," *Bioorganic and Medicinal Chemistry Letters*, vol. 17, no. 15, pp. 4258–4261, 2007.

[114] K. E. Hevener, R. Pesavento, J. Ren, H. Lee, K. Ratia, and M. E. Johnson, "Hit-to-Lead: hit validation and assessment," *Methods in Enzymology*, vol. 610, pp. 265–309, 2018.

[115] S. A. Hollingsworth and R. O. Dror, "Molecular dynamics simulation for all," *Neuron*, vol. 99, no. 6, pp. 1129–1143, 2018.

[116] M. Karplus and J. Kuriyan, "Molecular dynamics and protein function," *Proceedings of the National Academy of Sciences*, vol. 102, no. 19, pp. 6679–6685, 2005.

[117] J. Farmer, F. Kanwal, N. Nikulsin, M. C. B. Tsilimigras, and D. J. Jacobs, "Statistical measures to quantify similarity between molecular dynamics simulation trajectories," *Entropy*, vol. 19, no. 12, pp. 646/1–646/17, 2017.

[118] Y. W. Dong, M. L. Liao, X. L. Meng, and G. N. Somero, "Structural flexibility and protein adaptation to temperature: molecular dynamics analysis of malate dehydrogenases of marine molluscs," *Proceedings of the National Academy of Sciences of the United States of America*, vol. 115, no. 6, pp. 1274–1279, 2018.

[119] V. Kant, P. kumar, R. Ranjan, P. Kumar, S. Vijayakumar, and S. Vijayakumar, "In silico screening, molecular dynamic simulations, and in vitro activity of selected natural compounds as an inhibitor of Leishmania donovani 3-mercaptopyruvate sulfurtransferase," *Parasitology Research*, vol. 121, no. 7, pp. 2093–2109, 2022.

[120] A. A. Zaki, A. Ashour, S. S. Elhady, K. M. Darwish, and A. A. Al-Karmalawy, "Calendulaglycoside A showing potential activity against SARS-CoV-2 main protease: molecular docking, molecular dynamics, and SAR studies," *Journal of Traditional and Complementary Medicine*, vol. 12, no. 1, pp. 16–34, 2022.

[121] M. Congreve and F. Marshall, "The impact of GPCR structures on pharmacology and structure-based drug design," *British Journal of Pharmacology*, vol. 159, no. 5, pp. 986–996, 2010.

[122] S. Z. Grinter and X. Zou, "Challenges, applications, and recent advances of protein-ligand docking in structure-based drug design," *Molecules*, vol. 19, no. 7, pp. 10150–10176, 2014.

[123] A. K. Bronowska, "Thermodynamics - interaction studies - solids, liquids and gases," *Thermodyn. - Interact. Stud.-Solids, Liq. Gases*, vol. 1, pp. 1–49, 2011.

[124] S. Kwofie, B. Dankwa, K. Enninful et al., "Molecular docking and dynamics simulation studies predict Munc18b as a target of mycolactone: a plausible mechanism for granule exocytosis impairment in buruli ulcer pathogenesis," *Toxins*, vol. 11, no. 3, pp. 1–17, 2019.